

Entanglement Dynamics in Monitored Systems and the Role of Quantum Jumps

Youenn Le Gal,¹ Xhek Turkeshi,^{1,2} and Marco Schirò¹

¹*JEIP, UAR 3573 CNRS, Collège de France, PSL Research University,
11, place Marcelin Berthelot, 75231 Paris Cedex 05, France*

²*Institut für Theoretische Physik, Universität zu Köln, Zùlpicher Strasse 77, 50937 Köln, Germany*

(Dated: December 22, 2023)

Monitored quantum many-body systems display a rich pattern of entanglement dynamics, which is unique to this non-unitary setting. This work studies the effect of quantum jumps on the entanglement dynamics beyond the no-click limit corresponding to a deterministic non-Hermitian evolution. We consider two examples, a monitored SSH model and a quantum Ising chain, for which we show the jumps have remarkably different effects on the entanglement despite having the same statistics as encoded in their waiting-time distribution. To understand this difference, we introduce a new metric, the statistics of entanglement gain and loss due to jumps and non-Hermitian evolution. This insight allows us to build a simple stochastic model of a random walk with partial resetting, which reproduces the entanglement dynamics, and to dissect the mutual role of jumps and non-Hermitian evolution on the entanglement scaling. We demonstrate that significant deviations from the no-click limit arise whenever quantum jumps strongly renormalize the non-Hermitian dynamics, as in the case of the SSH model at weak monitoring or in the Ising chain at large transverse field. On the other hand, we show that the weak monitoring phase of the Ising chain leads to a robust sub-volume logarithmic phase due to weakly renormalized non-Hermitian dynamics.

I. INTRODUCTION

The spreading of quantum entanglement under unitary dynamics displays remarkable robustness and universality [1–3]. For example, in clean systems with short-ranged interactions, the entanglement entropy is generally expected to grow linearly in time and to saturate to a volume law [4, 5]; the violation of this behavior is often taken as a smoking gun of non-ergodic dynamics [6]. On the other hand, non-unitary processes such as quantum measurements can strongly affect how entanglement spreads throughout the system. Out of this competition, a novel type of measurement-induced phase transition (MIPT) in the entanglement content of the system has been discovered [7–9].

Entanglement transitions due to measurements have been studied broadly in two somewhat different settings. On the one hand, the stochastic dynamic encoded in a quantum many-body trajectory describes the system’s evolution conditioned to a set of measurement outcomes. A crucial aspect of this criticality is that it is hidden in the rare fluctuations of the measurement process, probed by non-linear functional of the state such as the entanglement entropy or the purity in a dynamical purification protocol [10], while conventional observables averaged over the noise are usually transparent to it. This makes the theoretical description and experimental detection of MIPT particularly challenging, even though recent progress has been made [11–13]. On the theoretical front volume-to-area law entanglement transitions have been reported in monitored random circuits [14–23] and non-integrable Hamiltonian [24–28] with projective or weak measurements. Monitored non-interacting systems, on the other hand, are not expected to sustain a volume law phase [29, 30]. Still, a critical sub-volume phase, whose origin and stability are currently under

debate [31–37], has been numerically found in several works [38–48].

A different limit of the measurement problem is obtained by post-selecting atypical trajectories corresponding to specific measurement outcomes. To fix the ideas, consider, for example, the quantum jump (QJ) dynamics corresponding to a photo-counting monitoring protocol [49–51]: here, abrupt random quantum jumps (clicks) intersperse the deterministic evolution driven by a non-Hermitian Hamiltonian, which accounts for the measurement back-action. Post-selecting on the trajectory where no click has happened corresponds to purely non-Hermitian dynamics. In this limit, several works have reported measurement-induced entanglement transitions and highlighted their relation with the spectral properties of the non-Hermitian Hamiltonian [52–63].

The relation between these two limits of the measurement problem, particularly concerning the entanglement dynamics, is not well understood. Is the no-click dynamics stable enough to include QJs, which should be seen as irrelevant perturbations? Or, on the contrary, do QJs completely change the entanglement structure of the monitored system? These questions ultimately go beyond measurement-induced transitions and touch upon the relevance of non-Hermitian Hamiltonians in the description of open quantum systems [64–67].

This work studies the quantum jumps dynamics of two monitored free-fermion models, the Su-Schrieffer-Heeger (SSH) model and the Quantum Ising chain. These models are attractive for two reasons: first, they differ in their global symmetry, a fact which is believed to play a critical role in the stability of the MIPT; second, their entanglement transition in the no-click limit has been studied in detail [55, 56]. By solving the full stochastic dynamics and computing the entanglement entropy, we show that QJs have remarkably different impacts on their respec-

tive phase diagram as compared to the no-click limit. This is particularly surprising as the two models share the same jump statistics, as we show by computing the QJs waiting-time distribution. To track down the origin of this difference we introduce a new metric that captures the effect of QJs on the entanglement. Specifically we compute the statistics of entanglement entropy changes after and in-between quantum jumps. We show that, on average, QJs induce an entanglement entropy loss while the non-Hermitian evolution causes a gain, although the statistics display rather broad tails and fluctuations.

Using this insight we introduce a classical stochastic random walk model with partial resetting, built-in using the full statistics of entanglement gain and loss, which is able to reproduce the full QJ dynamics of entanglement entropy for both models. More importantly, the entanglement gain and loss picture clarifies the mutual role of quantum jumps and non-Hermitian evolution in the scaling of entanglement entropy. Our analysis reveals that a crucial role of quantum jumps is to *renormalize* the effective non-Hermitian dynamics with respect to the bare no-click limit. We show that this renormalization, or its lack thereof, can naturally explain the different behaviors of quantum jumps in the two models and provide a criterion for the relevance of the no-click limit. Our results suggest a form of universality in how quantum jumps affect entanglement, providing a framework for interpreting the stochastic many-body dynamics in Hilbert space, which opens up to several applications.

The paper is structured as follows. In Sec. II we present a summary of the main results of this work. In Sec. III we review the background material: we introduce the QJ measurement protocol and the models we will consider throughout this work as well as the quantities we will use to characterize them. In Sec. IV we present our numerical results for the entanglement dynamics of the monitored SSH and Ising chain. In Sec. V we present our results for the waiting time distribution of quantum jumps. In Sec. VI we introduce our new metric, the statistics of entanglement gain and loss and describe a classical stochastic model for the entanglement dynamics. In Sec. VII we use the insights from this model to discuss the role of jumps and non-Hermitian dynamics on the scaling of the entanglement and the MITP. Finally Sec. VIII contains our conclusions and future perspectives. In the Appendixes we provide further methodological details and results relevant for our work.

II. OVERVIEW

In this Section, we summarize the main results of this work. We consider the entanglement dynamics of two models of non-interacting monitored fermions (See Fig. 1 (a) for a sketch), the Su-Schrieffer-Heeger (SSH) chain and the Quantum Ising chain, in the presence of Quantum Jump (QJ) monitoring. These models, in their no-click limit, feature a rich phase diagram with entangle-

ment transitions separating a volume (SSH)/sub-volume (Ising) entanglement phase at weak monitoring from an area law phase at strong monitoring [55, 56]. In Sec. IV, we compute the entanglement entropy under full stochastic monitoring dynamics and show that the effect of QJs is remarkably different for the two models. Specifically, we show that jumps in the SSH model have a substantial impact and qualitatively change the phase diagram with respect to the no-click limit. This fact is particularly manifest at weak monitoring, where the volume law phase is turned into a much less entangled, possibly logarithmic, phase. Such a phase eventually turns into an area law phase above a critical monitoring strength, whose value is also strongly renormalized by the jumps. In the Ising chain, on the other hand, our results show that QJs modify mainly quantitatively the no-click phase diagram and overall appear to be less of a relevant perturbation, except at large values of the transverse field, even though compelling differences emerge between the two phase diagrams.

In Sec. V, to understand the origin of such a different impact of QJs on the dynamics of the two models, we study the statistics of quantum jumps, particularly their waiting time distribution. The statistics of waiting times, which is naturally accessible using a higher-order Montecarlo wave function scheme, gives information on the typical time scale between jumps, *i.e.*, the time scale during which the non-Hermitian evolution is at play (See Fig. 1 (b)). Surprisingly, in both models, QJs at long times approach a Poisson distribution of waiting times with the same average waiting time. This analysis suggests that the difference observed in the entanglement dynamics does not arise from how jumps are distributed in time.

To proceed further, we introduce a new metric, namely the statistics of the changes to the entanglement entropy after and in between QJs. Specifically, we consider the stochastic dynamics of the entanglement entropy along a quantum trajectory (See Fig. 1 (b)) : the typical pattern is given by an evolution driven by the non-Hermitian Hamiltonian interrupted abruptly by a discontinuous change in entanglement entropy due to a quantum jump. The entanglement entropy can either increase or decrease after a jump and, similarly, can either grow or diminish during the time between the jumps, where non-Hermitian evolution occurs. Given this pattern, we now ask : what is the statistics of the entanglement entropy change after a quantum jump and after an evolution with the non-Hermitian Hamiltonian ? To answer this question, we sample the joint probability of observing a change ΔS_{qj} due to the jumps or δS_{nh} due to the non-Hermitian evolution (see inset of Fig. 1 (b)) together with a particular value of entanglement entropy S , *i.e.*, $P(\Delta S_{\text{qj}}, S)$, $P(\delta S_{\text{nh}}, S)$ which are obtained by binning stochastic events (jumps or non-Hermitian evolution) according to the *entanglement content* of the state they act on (which means the entanglement of the state before the event happens). The resulting histograms, plotted in

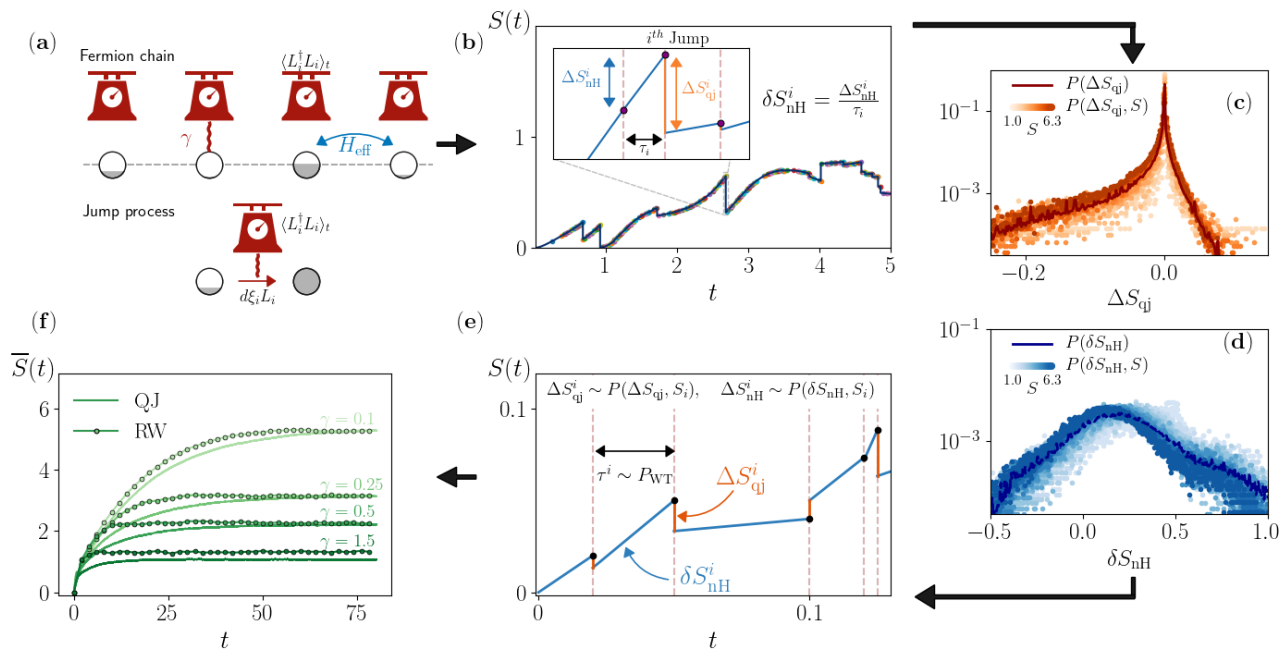


Figure 1: Panel (a) cartoon of the setup. A monitored fermionic chain evolving under quantum jump protocol. Panel (b): A quantum trajectory we obtain from this type of setup. The dots symbolize the jumps, and the inset shows how the quantities ΔS_{qj} (resp. ΔS_{nH}) are extracted from the change of entanglement happening in a jump (resp. during the non-Hermitian evolution). We define the effective slope δ_{nH} of the entanglement due to the non-Hermitian evolution between two consecutive jumps. The local entanglement S at which these events happen is stored to plot the joint probability of the following panels (c-d). In panel (c) is plotted in plain line the distribution of ΔS_{qj} , and the dots represent the joint version of this distribution with respect to the entanglement when the jumps is happening. In panel (d) we use the same typology but plotting this time the quantity δS_{nH} which is the effective non-Hermitian slope defined before. Panel (e): Cartoon depicting the entanglement dynamics as a classical random walk (RW) with stochastic drift and resetting drawn from the histograms in panels (c-d). Panel (f): Comparison between the dynamics of the average entanglement entropy obtained from the exact quantum jump dynamics (QJ) or the phenomenological classical random walk (RW).

Fig. 1 (c-d) for the Ising chain, are strongly asymmetric confirming the intuition that QJs induce on average an entanglement loss, while the non-Hermitian dynamics an entanglement gain, as we discuss in Sec. VI. Furthermore they feature broad tails which depend strongly on the entanglement content of the system, indicating for example that highly entangled states are more fragile to QJs.

Using the full statistics of entanglement changes we propose in Sec. VI a classical stochastic model (See Fig. 1 (e)) to understand the entanglement dynamics as a random walk with drift and partial resetting [43, 68, 69]. Within this model the probability of having an entanglement entropy S at time t , that we note $\mathcal{P}_t(S)$, evolves according to the master equation

$$\begin{aligned} \mathcal{P}_{t+dt}(S) = & rdt \int_{\Delta S_{\text{qj}}} P(\Delta S_{\text{qj}}, S - \Delta S_{\text{qj}}) \mathcal{P}_t(S - \Delta S_{\text{qj}}) + \\ & + (1 - rdt) \int_{\delta S_{\text{nH}}} P(\delta S_{\text{nH}}, S - \delta S_{\text{nH}}) \mathcal{P}_t(S - \delta S_{\text{nH}}) \end{aligned} \quad (1)$$

where the first term describes the jump, which adds a random contribution ΔS_{qj} with probability $rdt \times$

$P(\Delta S_{\text{qj}}, S - \Delta S_{\text{qj}})$, with r the resetting rate, while the second one describes the non-Hermitian dynamics which increase the entanglement of a random slope δS_{nH} with probability $(1 - rdt) \times P(\delta S_{\text{nH}}, S - \delta S_{\text{nH}})dt$. Using this classical stochastic model, we can reproduce accurately the dynamics of the average entanglement entropy as a function of the monitoring rate (See Fig. 1 (f) for the Ising chain).

In Sec. VII we use the insights obtained from our stochastic model to analyze the results for the entanglement in the two models and clarify the role of QJs and non-Hermitian evolution in the scaling of the steady-state entanglement entropy. Our analysis reveals, for example, that the logarithmic phase for the monitored SSH chain is mainly due to quantum jumps. At the same time, the non-Hermitian dynamics is strongly renormalized compared to the no-click limit. On the other hand, for the Ising chain at small values of monitoring rate and field, we see a logarithmic phase arising from both jumps and non-Hermitian evolution, the latter appearing to be only weakly renormalized with respect to the no-click limit. Upon increasing the transverse field or the monitoring rate, however, we find evidence of a strong renormaliza-

tion of the non-Hermitian dynamics due to the jumps, which explains the observed departure from the no-click limit. We conclude our analysis in Sec. VII by discussing the implications of our findings for the MIPT of free fermions.

III. BACKGROUND

In this Section, we summarize relevant background material, including the description of the Quantum Jump protocol and its sampling via the Montecarlo Wave Function and the Waiting Time-Distribution, and introduce the models we focus on throughout the paper and the methods to solve their dynamics. Finally, we recall their entanglement transition in the no-click limit and put that in the light of known results of monitored fermions.

A. Monitoring by Quantum Jumps

We start from the general Quantum Jump protocol for a given set of Kraus operators $\{M_\alpha\}$, for which $\sum_{\alpha \geq 0} M_\alpha M_\alpha^\dagger = \mathbb{1}$ [51, 70]. The evolution preserves the purity and is given by

$$|\psi(t+dt)\rangle = \sum_{\alpha \geq 0} d\xi_\alpha \frac{M_\alpha |\psi(t)\rangle}{\sqrt{\langle \psi(t) | M_\alpha^\dagger M_\alpha | \psi(t) \rangle}} \quad (2)$$

where $d\xi_0 \equiv (1 - \sum_{\alpha > 0} d\xi_\alpha)$, while, for $\alpha > 0$, $d\xi_\alpha \in \{0, 1\}$ is an increment for the inhomogeneous Poisson process with average $P(d\xi_\alpha = 1) = \langle \psi(t) | M_\alpha^\dagger M_\alpha | \psi(t) \rangle$. At infinitesimal times dt , the Kraus operators are expressed in terms of the Hamiltonian H and of jump operators $\{L_\alpha\}$ as $M_0 = 1 - dt(iH + \frac{1}{2} \sum_{\alpha > 0} L_\alpha^\dagger L_\alpha)$ and $M_\alpha = \sqrt{dt} L_\alpha$. We note that the $\frac{1}{2} \sum_{\alpha > 0} L_\alpha^\dagger L_\alpha$ in M_0 is imposed by the normalization condition. It is then possible to obtain a Stochastic Schrödinger Equation using Itô calculus ($d\xi_\alpha \propto \sqrt{dt}$, $d\xi_\alpha M_0 = d\xi_\alpha + o(dt)$) and keeping first order terms in dt , which reads [49, 50, 71]

$$d|\psi(t)\rangle = -idt \left\{ H - \frac{i}{2} \sum_{\alpha > 0} (L_\alpha^\dagger L_\alpha - \langle L_\alpha^\dagger L_\alpha \rangle_t) \right\} |\psi(t)\rangle + \sum_{\alpha > 0} d\xi_\alpha \left\{ \frac{L_\alpha}{\sqrt{\langle L_\alpha^\dagger L_\alpha \rangle}} - 1 \right\} |\psi(t)\rangle. \quad (3)$$

This last equation is composed of a deterministic part which corresponds to an effective non-Hermitian Hamiltonian H_{eff} given by

$$H_{\text{eff}} = H - \frac{i}{2} \sum_{\alpha > 0} L_\alpha^\dagger L_\alpha \quad (4)$$

and a stochastic one due to the action of quantum jumps. The effective Hamiltonian is not Hermitian because of

the back-action of the jumps and corresponds to the no-click limit, where no jumps happen during the trajectory. We note that the evolution of the system is state-dependent (thus nonlinear); see the counter-term appearing in Eq. (3), to ensure the normalization.

B. Monte Carlo Wave Function and Waiting Times

The stochastic Schrödinger equation (3) is solved via Monte Carlo methods [71], which we briefly review below starting from the first-order integration schemes. In this case, the idea is to divide the time evolution into segments of interval dt , and act on the system accordingly to the probability of having a quantum jump $P_{\text{Jump}} \equiv \sum_{\alpha > 0} P(d\xi_\alpha = 1)$ or evolving under the non-Hermitian Hamiltonian $P_{\text{nH}} \equiv 1 - P_{\text{Jump}}$. At a sufficiently small time interval dt , the probability of a jump P_{Jump} is small, since $P(d\xi_\alpha = 1) = dt \langle \Psi(t) | L_\alpha^\dagger L_\alpha | \Psi(t) \rangle$ with $\alpha > 0$. If a jump occurs, we divide the interval $[0, 1]$ into segments of length $P(d\xi_\alpha = 1)/P_{\text{Jump}}$. The jump channel $\tilde{\alpha} > 0$ is selected checking in which subinterval a uniformly drawn random number falls. Then, the measurement is assumed to occur in dt time, and leads to

$$|\Psi(t+dt)\rangle = \frac{L_{\tilde{\alpha}} |\Psi(t)\rangle}{\sqrt{\langle \Psi(t) | L_{\tilde{\alpha}}^\dagger L_{\tilde{\alpha}} | \Psi(t) \rangle}}. \quad (5)$$

If no jump occurs, the state is given by

$$|\Psi(t+dt)\rangle = \frac{(1 - iH_{\text{eff}} dt) |\Psi(t)\rangle}{\sqrt{P_{\text{nH}}}} = \frac{|\tilde{\Psi}(t)\rangle}{\sqrt{P_{\text{nH}}}} \quad (6)$$

This process is the implementation of the POVM described before (cf. Eq. (2)) with a finite dt . We note that $P_{\text{nH}} = 1 - P_{\text{Jump}}$ is due to

$$\begin{aligned} \langle \tilde{\Psi}(t) | \tilde{\Psi}(t) \rangle &= 1 - dt \langle \Psi(t) | i (H_{\text{eff}} - H_{\text{eff}}^\dagger) | \Psi(t) \rangle \\ &= 1 - dt \sum_{\alpha > 0} \langle \Psi(t) | L_\alpha^\dagger L_\alpha | \Psi(t) \rangle = 1 - P_{\text{Jump}} \end{aligned} \quad (7)$$

which is a consequence of the normalisation of the Kraus operators in the POVM [51, 70]. This procedure has the drawback of not having a natural way to control the accuracy of the simulation, which is instead empirically benchmarked by considering different choices of dt and checking that there is not qualitative difference in disorder averages.

We overcome these limitation considering a higher-order scheme that is based on sampling the time at which subsequent jumps happen [70, 71], i.e., using the cumulative waiting-time distribution defined as

$$F[\Psi, \tau] = 1 - \langle \Psi | e^{iH_{\text{eff}}^\dagger \tau} e^{-iH_{\text{eff}} \tau} | \Psi \rangle. \quad (8)$$

Specifically, we proceed by iterating the following loop : (i) Assume a normalised state $|\Psi(t_i)\rangle$ is reached at time t (possibly the initial time of the dynamics, in which case

$|\Psi(t)\rangle$ is the initial state). (ii) Extract a random number r uniformly distributed in $[0, 1]$ and find the random waiting time τ for the next jump by solving the equation $r = 1 - F[\Psi(t), \tau]$.

(iii) Within the time interval $[t, t + \tau]$ propagate the deterministic non-Hermitian evolution

$$|\Psi(t + \tau)\rangle = \frac{e^{-iH_{\text{eff}}\tau}|\Psi(t)\rangle}{\|e^{-iH_{\text{eff}}\tau}|\Psi(t)\rangle\|}. \quad (9)$$

(iv) At time $t + \tau$ a quantum jump occurs. As before, the output channel is chosen splitting the $[0, 1]$ interval into segments of size $\langle\Psi(t + \tau)|L_{\alpha}^{\dagger}L_{\alpha}|\Psi(t + \tau)\rangle$ and checking in which one a uniformly drawn random number falls. The jump is immediate and the post-measurement state is

$$|\Psi(t + \tau^+)\rangle = \frac{L_{\bar{\alpha}}|\Psi(t + \tau)\rangle}{\sqrt{\langle\Psi(t + \tau)|L_{\bar{\alpha}}^{\dagger}L_{\bar{\alpha}}|\Psi(t + \tau)\rangle}}. \quad (10)$$

In a nutshell, a quantum trajectory is specified as a sequence of non-Hermitian quantum quenches interspersed with discontinuous jumps, that set the initial conditions for the forthcoming integration steps.

An advantage of this approach is to access directly the waiting-time distribution (WTD) or delay function [71–73]. We will discuss the behavior of the waiting time distribution for the models of interest later on. In general, computing the waiting time distribution is non-trivial and requires the knowledge of the stochastic process. There is, however, a special case where this can be done. Whenever the imaginary part of the non-Hermitian Hamiltonian commutes with the real part, then one can conclude that the norm decay is exponential and therefore so the cumulative waiting time-distribution, $F = 1 - \exp(-\Gamma\tau)$. In this case, the time for the next jump can be directly obtained as a function of a random number r , as $\tau = -\frac{1}{\Gamma}\ln r$. Such an instance occurs for a system with local density monitoring and conservation of global particle number [31, 38].

C. Average vs Conditional Dynamics and Entanglement Entropy

In the following we will be interested in the conditional jump dynamics described by the stochastic Schrödinger equation (3) and in particular in the entanglement dynamics of the conditional state, also called a quantum trajectory. Indeed, it is known that by averaging the density matrix over the stochastic noise in Eq. (3) one recovers a Lindblad master equation, which describes in the present context heating towards a trivial infinite temperature state. In the following we will be mainly interested in the (von Neumann) entanglement entropy, defined as [74, 75]

$$S(\xi_t) = -\text{tr}_A [\rho_A(\xi_t) \ln \rho_A(\xi_t)], \quad (11)$$

where we have introduced a partition $A \cup B$ and the reduced density matrix $\rho_A(\xi_t) = \text{tr}_B |\Psi(\xi_t)\rangle\langle\Psi(\xi_t)|$. In particular we will focus on the conditional average entanglement entropy, given by

$$\bar{S}(t) = \int \mathcal{D}\xi_t P(\xi_t) S(\xi_t). \quad (12)$$

Additionally, we will also discuss the statistics of local observables, in particular of the operator that is monitored by the measurement process. Setting $\langle O \rangle_{\xi} \equiv \langle\Psi(\xi)|O|\Psi(\xi)\rangle$, we are interested in the probability distribution function [52, 76–78]

$$P_t(O; o) = \int \mathcal{D}\xi_t P(\xi_t) \delta(\langle O \rangle_{\xi} - o), \quad (13)$$

which is as a highly non-linear functional of ρ_{ξ} and, therefore, beyond the reach of the Lindbladian formalism.

D. Models

In the following we consider two models of monitored free fermions (See Fig. 1 a). The first model is a fermionic Su-Schrieffer-Heeger (SSH) chain with two different sublattices A and B and Hamiltonian

$$H_{\text{SSH}} = - \sum_{j=1}^L \left[(J - h) c_{A,j}^{\dagger} c_{B,j-1} + (J + h) c_{A,j}^{\dagger} c_{B,j} + \text{h.c.} \right]. \quad (14)$$

We choose the jump operators as

$$L_{A,i} = \sqrt{2\gamma} n_{A,i} \quad L_{B,i} = \sqrt{2\gamma} (1 - n_{B,i}), \quad (15)$$

namely we independently and continuously monitor the local density of particles on sublattice A , $n_{A,i} = c_{A,i}^{\dagger} c_{A,i}$, and the local density of holes, $1 - n_{B,i} = c_{B,i} c_{B,i}^{\dagger}$, on sublattice B . Using these quantum jump operators we obtain an effective non-Hermitian Hamiltonian of the form

$$H_{\text{eff}} = H_{\text{SSH}} - i\gamma \sum_{i=1}^L (c_{A,i}^{\dagger} c_{A,i} + c_{B,i} c_{B,i}^{\dagger}). \quad (16)$$

where the normalization can be taken into account by adding the counterterms as in Eq. 3 above. The entanglement dynamics generated by this model, evolving deterministically under H_{eff} and properly normalized, has been studied in detail in Ref. [56] (see later for a summary).

The second model is the Quantum Ising chain in a transverse field

$$H_{\text{Ising}} = - \sum_{i=1}^L [J \sigma_i^x \sigma_{i+1}^x + h \sigma_i^z] \quad (17)$$

which is mapped via a Jordan Wigner transformation to

$$H_{\text{Ising}} = - \sum_{i=1}^L [J (c_i^{\dagger} c_{i+1} + c_i^{\dagger} c_{i+1}^{\dagger} + \text{h.c.}) + h(1 - 2n_i)]. \quad (18)$$

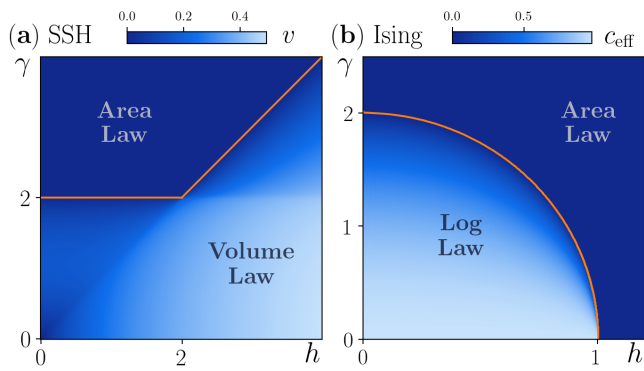


Figure 2: Entanglement phase diagram of the monitored SSH and Ising models in the no-click limit, corresponding to a deterministic non-Hermitian evolution with H_{eff} . Left panel: non-Hermitian SSH and volume-to-area-law transition [56]; Right panel: non-Hermitian Ising chain, featuring a transition from a critical phase with logarithmic scaling of the entanglement to an area law Zeno phase [55]. Note that our convention for the jump operators in Eq. (19) leads to a rescaling of γ by a factor $1/2$, with respect to Ref. 55.

We choose the jump operators

$$L_i = \sqrt{2\gamma}n_i, \quad (19)$$

and get the effective non-Hermitian Hamiltonian

$$H_{\text{eff}} = H_{\text{Ising}} - i\gamma \sum_i n_i. \quad (20)$$

Also for this non-Hermitian model the entanglement dynamics has been studied in detail and obtained in closed form in the thermodynamic limit in Ref. [55]. We will discuss in Sec. IV the effect of QJs.

E. Summary of Entanglement Dynamics in the No-Click Limit

Here we briefly review the results obtained for the dynamics of the entanglement entropy under purely non-Hermitian evolution driven by H_{eff} , both for the SSH and for the Ising model, corresponding to the no-click limit of the QJ dynamics. In both cases the time evolution for the entanglement entropy $S_{\text{nH}}(t)$ can be computed exactly in the thermodynamic limit using free-fermion techniques [55, 56]. The results have revealed a rich phase diagram as a function of the monitoring strength γ , which for a non-Hermitian problem is given by the back-action term, and the field h entering the non-Hermitian Hamiltonian. We plot in Fig. 2 the phase diagram of the two models for completeness.

In the non-Hermitian SSH model in Eq. (16) the weak monitoring phase for $\gamma < \gamma_c^{\text{SSH}}(h)$ is characterized by an entanglement entropy growing linearly in time, $S_{\text{nH}}(t) \sim t$ and saturating to a stationary value that scales linearly with the subsystem size ℓ , i.e.,

$S_{\text{nH}}(t \rightarrow \infty) \simeq v\ell$, characteristic of a volume-law phase. This is associated to the purely real spectrum protected by PT symmetry [56]. The close-form expression of v allows the complete characterization of the entanglement phases. As the measurement strength γ increases at fixed h the prefactor v of the volume law scaling decreases (cf. Fig. 2(a)) until a critical value is reached when $v = 0$ and the system enters the area-law scaling for the entanglement entropy. This entanglement transition was shown to be directly related to the spectral transition occurring in H_{eff} [56]. At weak monitoring the non-Hermitian quasiparticle spectrum is purely real due to the PT symmetry of H_{eff} and as γ increases first PT breaks and some quasiparticle mode acquires a finite-lifetime, which induces a sharp decrease of v . However it is only at $\gamma_c^{\text{SSH}}(h)$, when all the quasiparticle modes acquire a finite lifetime, the system enters the area-law scaling for the entanglement entropy.

In the non-Hermitian Ising chain in a complex transverse field, Eq. (20), the entanglement entropy was found for weak monitoring $\gamma < \gamma_c^{\text{Ising}}(h)$ to depend logarithmically on both time and subsystem size. The corresponding effective central charge c_{eff} , obtained from the ansatz $S_{\text{nH}}(\ell) = c_{\text{eff}} \ln(\ell)$, could be obtained in closed form [55] and was shown to decrease as a function of both γ and h up to the critical line $\gamma_c^{\text{Ising}}(h)$, above which the system was found to undergo an entanglement transition into an area-law phase, cf. Fig. 2(b). As for the SSH case, the entanglement transition for the Ising chains is directly related to a transition in the spectrum of non-Hermitian quasiparticles. The latter separates a critical gapless phase with vanishing imaginary part of the spectrum at a given point in the Brillouin zone, from a gapped phase [52]. In the next sections, we will discuss how the presence of quantum jumps modify the entanglement dynamics in these two models.

F. Relation to Prior Works

Here we position our work with respect to the current literature on monitored quantum systems. Non-interacting systems in particular have been discussed extensively, both numerically and analytically. Free fermions with global $U(1)$ symmetry, related to charge conservation at the single trajectory level, were shown to display a transition from a critical phase logarithmic scaling of entanglement entropy to an area-law for both quantum-jumps and quantum state diffusion (QSD) type of density-monitoring [38, 39]. A related transition was also found in the entanglement negativity in presence of boundary driving [79]. Our monitored SSH model falls a priori in the same class, since the global charge is conserved at the trajectory level, even though the monitored observable is not the total density which introduces some differences as we will discuss. This entanglement transition was first interpreted as a Kosterlitz-Thouless criticality based on a two-replica

field theory and bosonization [80]. The robustness of the weak-monitoring sub-volume phase, and hence of the transition, was questioned in the case of projective measurements, where numerical evidence supported an area-law steady-state entanglement [31]. This result has been theoretically understood within a replica field theory calculation [33] which identified connections with the physics of weak-localisation corrections in Anderson localisation. Later work has extended this analysis to higher-dimensions [81], finding a stable entanglement transition, as parallelly done within the QSD protocol, where non-trivial connections to multifractality were highlighted [82].

When the symmetry is reduced to a discrete Z_2 , corresponding to our Ising chain or Majorana fermions, a logarithmic to area law transition has been found both under QSD [40, 44] and QJ [41, 43, 46]. In the latter case a phenomenological quasiparticle picture connected the latter to the no-click limit [43]. The replica field theory analysis, applied to a circuit model with temporal randomness and QSD monitoring also pointed towards a transition [34], although with a different scaling of the entanglement [32, 35].

With respect to those works we emphasize that the QJ protocol we consider here differs in one key aspect, namely noise distribution is state-dependent a priori and not prefixed, which makes the averaging over the noise, required to construct the replica field theory, non-trivial. Finally, for interacting systems QJ monitoring has been explored and shown to lead to a volume-to-area law transition [24].

IV. ENTANGLEMENT DYNAMICS UNDER QUANTUM JUMPS

In this section we present our results for the QJ dynamics of the SSH and Ising chain model, focusing first on the dynamics of the entanglement entropy. Unless specified otherwise, throughout this section we consider an initial product state of the form $|\Psi(0)\rangle = |0, 1, 0, 1, \dots, 0, 1\rangle$ and open boundary conditions. We fix the hopping along the chains as units of energy and inverse time, $J = 1$. We integrate the dynamics with a time-step $dt \propto 1/(4\gamma L)$. Throughout this work we consider a system of size $L = 128$.

A. Entanglement Dynamics in the Monitored SSH Model

We start discussing the entanglement dynamics for the monitored SSH. In Fig. 3 (a-c), we show the evolution of the entanglement entropy for a sample of quantum trajectories for increasing values of the monitoring rate $\gamma = 0.5, 1.5, 2.5$, corresponding to the volume-law [panels (a,b)] and area-law [panel (c)] phase of the no-click limit, cf. Fig. 2. For comparison, we also plot

the average entanglement entropy (obtained averaging over the different trajectories, according to Eq. (12)) as well as the value obtained in the non-Hermitian no-click limit. We see that, for weak monitoring, when the no-click dynamics displays a linear growth corresponding to the volume law phase, the stochastic dynamics due to quantum jumps suppress the entanglement very effectively and bring the system to a stationary state which is less entangled than in the no-click limit. In this regime, an agreement with pure non-Hermitian evolution is present only for short periods of time. We also notice that for weak monitoring, trajectory-to-trajectory fluctuations are rather broad, and certain outliers follow the non-Hermitian evolution for longer times before ultimately deviating from it. On the other hand, in the regime of strong monitoring, when the non-Hermitian dynamics display an area law behavior, the role of quantum jumps is less drastic. While we still see strong fluctuations, the average entanglement entropy follows the no-click limit rather closely all the way to the stationary state. From these first results, we can already anticipate that QJs will have a disruptive effect on the volume law phase of the non-Hermitian SSH model. This can be understood by considering that the stochastic noise due to the jumps breaks the PT-symmetry of the non-Hermitian SSH model, which played a major role in protecting the volume law phase in the no-click limit [56].

To better characterize the entanglement content in the jump dynamics, we consider the long-time steady state and study the scaling of the average entanglement entropy with the subsystem size ℓ as a function of the measurement rate γ . In Fig. 3 (d), we show that in the weak-monitoring regime, the volume law scaling of the no-click evolution is substituted by a much slower scaling compatible with a logarithmic growth, which eventually gives away for an area law phase upon increasing γ . Following the literature on monitored free fermions [38, 40, 43] we can use the phenomenological fit

$$S_\ell^\infty = c_{\text{eff}} \log \ell \quad (21)$$

to obtain an estimate for the prefactor c_{eff} , sometime called effective central charge c_{eff} . As we show in the panels (e) and (d) of Fig. (3), this quantity vanishes as a function of both γ and h , indicating a transition into an area-law phase. As we see from panel (e), this transition occurs for values of $\gamma \simeq 1$, i.e., still within the volume law phase of the no-click problem (See Fig. 2). Furthermore, the critical point γ_c decreases weakly for $h < 2$, as opposed to the no-click result. On the other hand, we note that the effective central charge is non-monotonous as a function of h , vanishing around $h \simeq 2$. This result can be understood from the fact that the band of non-Hermitian Hamiltonian becomes flat around that value [56]. We emphasize that the transition between log and area law scaling could well turn into a crossover upon increasing system sizes through a weak-localization mechanism similar to what was recently discussed in the case of free fermions with $U(1)$ symmetry and projective

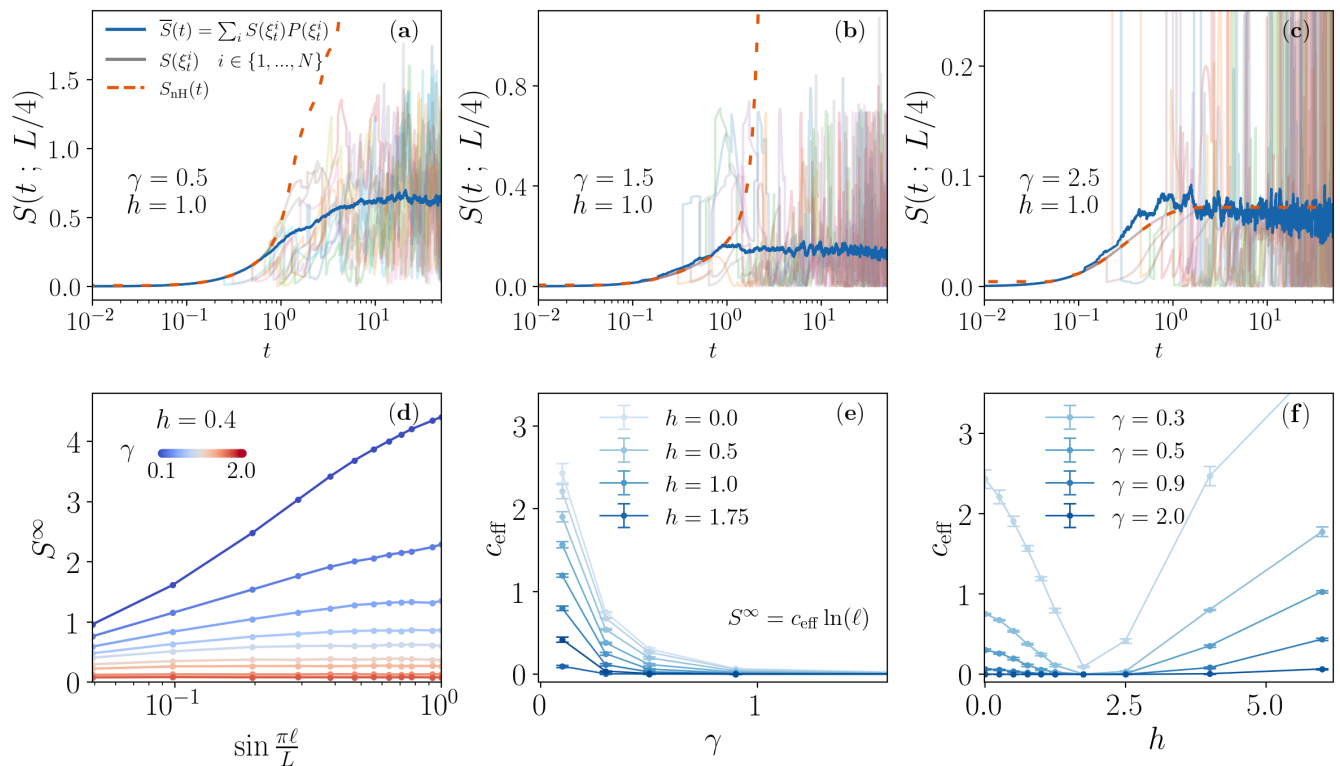


Figure 3: Entanglement dynamics under QJ monitoring for the SSH chain — (a-c) Comparison between average, trajectory and no-Click evolution for different values of the measurement rate $\gamma = 0.5, 1.5, 2.5$. (d) Average steady-state entanglement for the monitored SSH model ($\gamma = \{0.1, 0.2, 0.3, 0.4, 0.5, 0.7, 0.9, 1.5, 2.0\}$). We see for weak monitoring a logarithmic scaling that evolves into an area law upon increasing γ ; Phase diagram as obtained from the effective central charge c_{eff} as a function of γ (e) and h (f).

measurements [33]. Although affected by the inevitable finite-size effects, our results show that the volume law phase of the non-Hermitian SSH is not stable when including quantum jumps. As compared with the phase diagram of the no-click limit, we see that not only does the volume-law turn into a logarithmic phase but also that the emerging area law phase is significantly more extended throughout the phase diagram, which is therefore qualitatively and quantitatively affected by the inclusion of quantum jumps.

B. Entanglement Dynamics in the Monitored Ising Chain

We now move to the monitored Ising chain and present our results for the entanglement entropy dynamics under QJs. These complete previous results obtained in Ref. [43, 46]. As done before for the SSH case, we start in Fig. 4 presenting the dynamics of the entanglement entropy for a certain number of stochastic trajectories and compare to the average value and the value obtained in the no-click limit.

As a first observation, we note that in the weak monitoring phase, $\gamma = 0.5$, $h = 0.4$ [panel (a)], the non-

Hermitian result follows quite closely the average entanglement entropy and the fluctuations appear to remain modest in size. At long times, we see a deviation, namely, the non-Hermitian dynamics reach a maximum and then decrease, while the QJs attain a stationary state value, which still contains fluctuations. As the value of the monitoring rate γ increases [cf. panel (b) for $\gamma = 1.5$, $h = 0.4$], we observe a similar trend, namely that quite generically, the agreement between no-click and QJs is good at short and intermediate times, while at long-times quantum jumps can stabilize a more entangled state than in the pure no-click non-Hermitian case.

After this qualitative discussion, we present in Fig. 4 (d-f) the scaling of the steady-state entanglement entropy as a function of the subsystem size ℓ , for different values of the parameters. In panel (d) we confirm that the weak monitoring phase has a logarithmic dependence of the entanglement entropy, which evolves into an area law upon increasing γ . Following previous works we extract an effective central charge c_{eff} by fitting a logarithmic scaling of the entanglement entropy in the steady state, cf. Eq. (21). In Fig. 4 (e,f) we plot this quantity as a function of γ and h . We see that increasing γ at fixed h drives a transition into an area law phase when $c_{\text{eff}} = 0$, in qualitative analogy to the no-click limit. The criti-

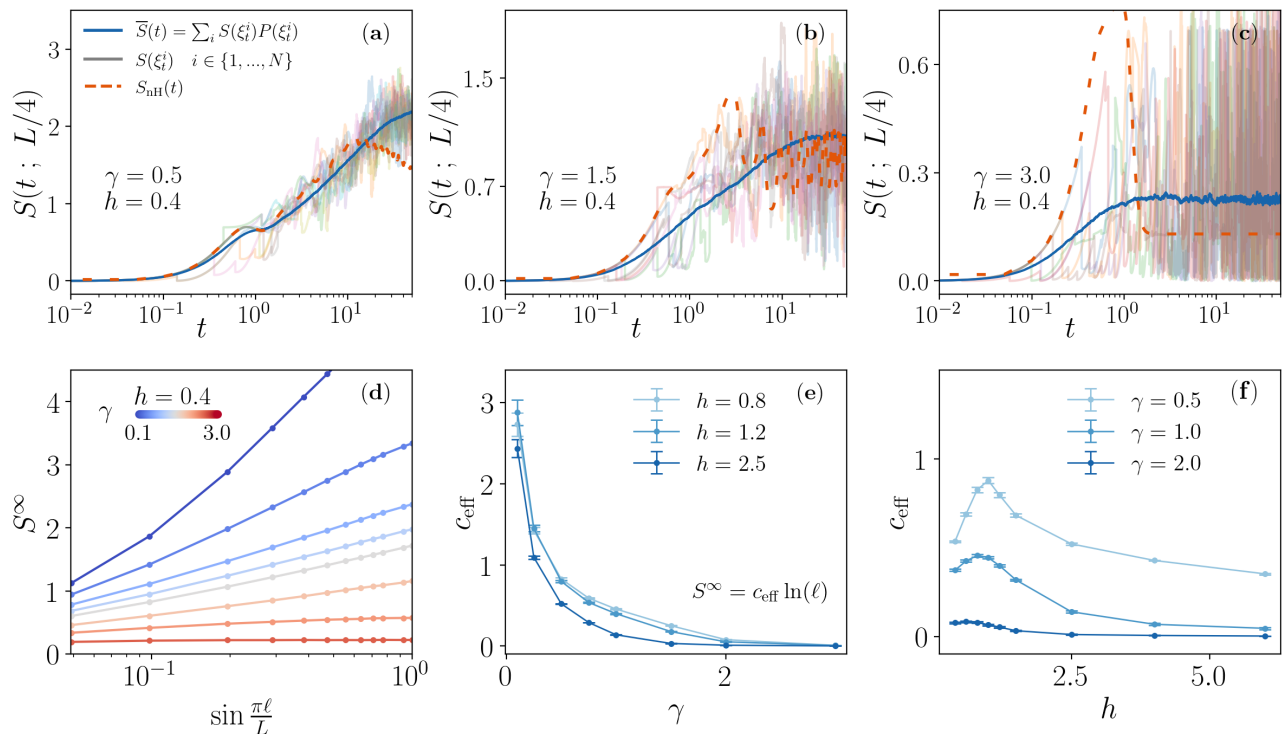


Figure 4: Entanglement dynamics under QJ monitoring for the Ising chain — (a-c) Comparison between average, trajectory, and no-click evolution for different values of the measurement rate $\gamma = 0.5, 1.5, 3.0$ and $h = 0.4$. (d) Average steady-state entanglement entropy ($\gamma = \{0.2, 0.5, 1.0, 1.5, 2.0, 3.0, 4.0, 6.0\}$). We see for weak monitoring a logarithmic scaling that evolves into an area law upon increasing γ ; Phase diagram as obtained from the effective central charge c_{eff} as a function of γ (e) and h (f).

cal point $\gamma_c(h)$ decreases weakly with the transverse field [see panel (e)], a result which is qualitatively similar to the no-click case where however this effect is more pronounced, cf. Fig. 2. If we instead fix the value of the monitoring rate and increase the transverse field h we see in panel (f) a rather different behavior: for small γ the effective central charge has a maximum and then decreases with h , while for larger values of γ we still see an effect similar to the no-click limit, with c_{eff} vanishing at a critical h . This has an interesting consequence, already noticed in Ref. [46], namely that for large $h > 1$ the monitored problem shows a sub-volume logarithmic scaling of the entanglement entropy in a region where according to the no-click evolution the system should be in the area law. Here we find similar results as we show in Fig. 4 (e,f): both at large $h > 1$ and at large $\gamma > 2.0$ the system still displays a finite $c_{\text{eff}} > 0$, while the no-click limit would predict an area law phase.

The outcome of this comparison confirms that, quite generally, the QJ dynamics in the Ising chain retain many features of the non-Hermitian phase diagram. However, the phase transition into the area law is renormalized concerning the no-click limit value. In particular, quantum jumps enhance the entanglement entropy to a logarithmic law in regions of the phase diagram where the no-click dynamics would predict an area law. These results high-

light a compelling difference between the SSH and Ising models. While the former QJs have severe effects on the weakly monitored phase, deteriorating the volume-law phase to a logarithmic phase, the latter QJs show a marked contribution in the area-law phase of the non-Hermitian Hamiltonian, cf. for a measurement-altered analysis [83, 84]. We will return to this point in Sec. VII.

To summarize, in this Section we have shown that QJs affect the dynamics of entanglement entropy in rather different ways for our two models. Similar conclusions can be drawn by looking at other non-linear functions of the state, e.g., the statistics of the monitored density, that we discuss in Appendix A. In the following sections, we will provide a theoretical framework to understand this difference and the deviations with the no-click limit.

V. STATISTICS OF QUANTUM JUMPS

The results of the previous Section have shown that QJs act as a strong perturbation concerning the dynamics of the non-Hermitian SSH, while they appear less relevant for the Ising chain. In particular, we have shown that the non-Hermitian dynamics leave their fingerprints on the stochastic evolution in the Ising case, while it appears to be washed away for the SSH model. In this Section, we

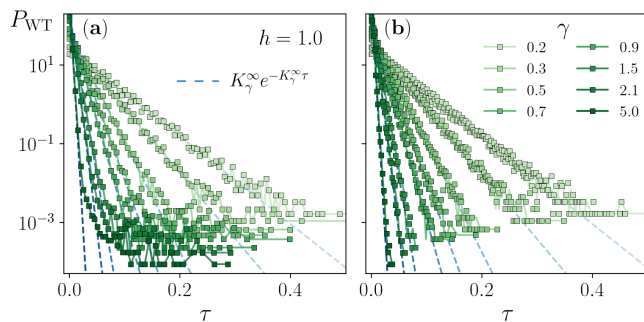


Figure 5: Waiting Time Distribution for the SSH model obtained numerically for different values of γ . In the left panel (a) the entire dynamics is considered whereas in the right panel (b) only QJs occurring in the long-time steady state are sampled. We see that in the latter case a clear Poisson law emerges, while short-time jumps are affected by the initial condition and display a longer average waiting time.

try to understand whether such a difference arises from different statistical properties of QJs in those two models. Indeed, one possible scenario to explain the different roles of quantum jumps could be that the statistics of quantum jumps become particularly broad and, as a consequence, jumps are rare and diluted, leaving more space for the non-Hermitian evolution to control the physics. As we will see in this Section, this naive expectation is incorrect.

To study how QJ are distributed in time, we compute their Waiting-Time Distribution (WTD). This quantity naturally emerges in the numerical implementation of stochastic QJ dynamics beyond the first-order Monte Carlo schemes [71]. Furthermore, WTDs have been studied in the early days of quantum jumps, motivated by resonance fluorescence spectra [72, 85], and have found a multitude of applications from solid-state quantum information [86] to quantum transport [73, 87–91] to laser cooling [92].

We start by discussing the SSH case for which we plot the WTD (obtained numerically) in Fig. 5. We note from panel (a) that the WTD displays an exponential decay typical of a Poisson law at weak monitoring. In contrast, upon increasing the monitoring rate, we see the development of nonexponential tails, giving rise to longer waiting times. This fact can partially explain the agreement between QJs and non-Hermitian dynamics at short times, see for example in Fig. 3. While the results in panel (a) have been obtained by sampling the jumps over full-trajectories, in panel (b), we consider only the jumps occurring at long times, i.e., in the steady state, for which we see a clear Poisson law emerging for all monitoring rates. We can better understand the origin of the tails in the short-time WTD by recalling that this distribution is controlled by the decay of the norm $\mathcal{N}(t) \equiv \|e^{-iH_{\text{eff}}t}|\Psi\rangle\|$, cf. Eq. (8), which reads in general $\mathcal{N}(t) = \exp(-K(t)t)$. In the case of the SSH model the observable $K(t)$ driving the decay of the norm is $K_{\text{SSH}}(t) = 2\gamma \sum_i [n_{A,i}(t) + 1 - n_{B,i}(t)]$, where

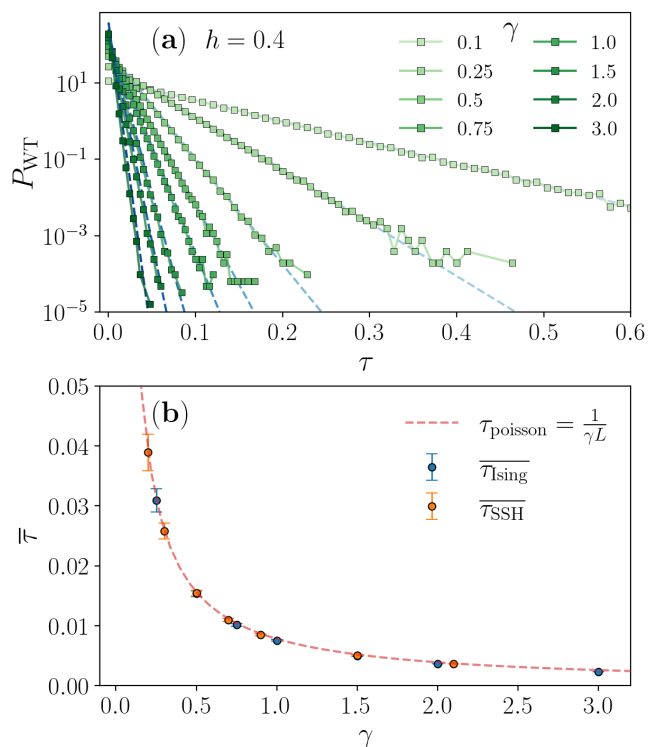


Figure 6: Waiting Time Distribution for the monitored Ising chain obtained numerically for different values of γ , showing a perfect agreement with a Poisson law. In the bottom panel, we compare the average waiting time of quantum jumps in the two models, showing perfect agreement. In both cases $\bar{\tau} \sim 1/\gamma L$.

$n_{A/B,i}(t) = \langle \Psi(t) | c_{A/B,i}^\dagger c_{A/B,i} | \Psi(t) \rangle$. At short times, the observable $K_{\text{SSH}}(t)$ displays significant temporal fluctuations due to the chosen initial condition, and the WTD shows longer tails. On the other hand, at long times one obtains a Poisson law

$$P_{WT}(\tau; t \rightarrow \infty) \sim e^{-K_\infty \tau} \quad (22)$$

whose average waiting time is scaling as $1/\gamma L$ and thus increases as γ decreases, cf. Fig. 6 (b). A Poisson distribution of QJ is typical for systems in which the backaction term is a constant of motion. In the SSH setup, this is not the case, and in fact, we note that this WTD is a property of the steady-state jump dynamics due to the observable $K(t \rightarrow \infty)$.

Similarly, we compute the WTD for the Ising chain ; see Fig. 6 (a). Even in this case, we find that jumps are distributed according to a Poisson law. To understand this result, it is important to recall that jumps try to refill empty sites and keep the total number of particles effectively constant. Thus, $K(t)$ is centered around the average number of particles with small fluctuations. Interestingly, both models feature the same average waiting time of QJs, as shown in Fig. 6 (b), and given by $\bar{\tau} \sim 1/\gamma L$.

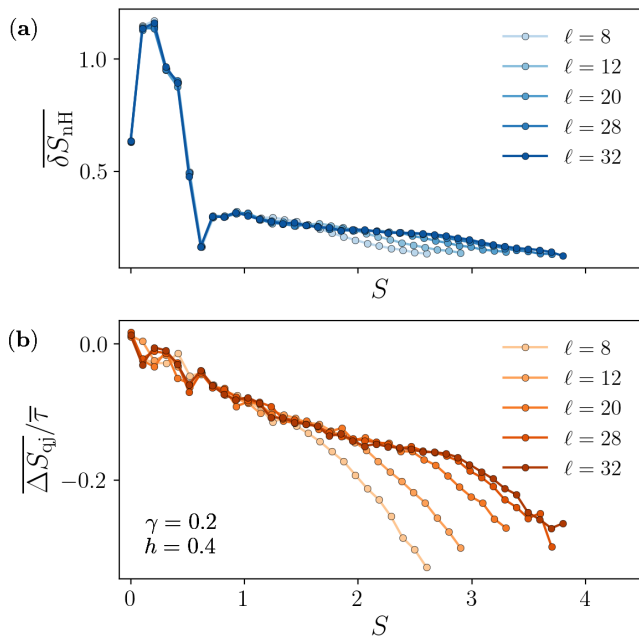


Figure 7: Average change to the entanglement entropy due to non-Hermitian evolution (panel a) and QJs (panel b). These averages are obtained from the joint distributions, $P(\Delta S_{\text{qj}}, S)$, $P(\Delta S_{\text{nh}}, S)$, thus are a function of the entanglement entropy S and we represent in these plots the dependence from subsystem size ℓ .

VI. STATISTICS OF ENTANGLEMENT GAIN AND LOSS

The study of the statistics of waiting times for quantum jumps discussed in the previous Section reveals a rather common pattern for the two models, namely, at long times, the WTD of the jumps flows towards a universal Poisson law, independent of the state, with an average waiting time $\bar{\tau} \sim 1/\gamma L$. This suggests that it is not the time distribution or the number of jumps that control their impact on the entanglement structure of the state. To better understand the intertwined role of QJs and non-Hermitian dynamics, we introduce a new metric that looks at the statistics of the change in entanglement entropy *after* and *in-between* quantum jumps. Specifically, we sample throughout a quantum trajectory (see Fig. 1 (b)) the changes in entanglement entropy at each jump event and in between the jumps (due to the non-Hermitian evolution) and repeat this sampling for different trajectories to collect two histograms $P(\Delta S_{\text{qj}})$ and $P(\delta S_{\text{nh}})$. We have plotted these histograms in Fig. 1 (c-d) for the monitored Ising chain. The first interesting observation is that the QJ distribution is strongly peaked around $\Delta S_{\text{qj}} = 0$ and has broad asymmetric tails, suggesting that the vast majority of quantum jumps do not substantially change the entanglement entropy. In contrast, rare quantum jumps are responsible for more significant changes, and this can be also observed at the

level of the trajectory in Fig. 1 (b). The asymmetry of the distribution is also interesting to note since it means that a single QJ is more likely to reduce the entanglement entropy, even though jumps that increase it are also possible. For what concerns the entanglement changes during the non-Hermitian evolution in between quantum jumps, we see that the distribution appears centered around a slightly positive value and with a slight asymmetry in the tails, suggesting that the non-Hermitian evolution is primarily responsible for the growth of the entanglement.

In the same plots in Fig. 1 (c-d) we also consider the joint probability of observing a change ΔS_{qj} (or δS_{nh}) in correspondence of a particular value of entanglement entropy S , i.e., $P(\Delta S_{\text{qj}}, S)$, $P(\delta S_{\text{nh}}, S)$ which are obtained by binning stochastic events (QJs or non-Hermitian evolution) according to the *entanglement content* of the state they act on. The key idea here is to understand whether QJs impact highly or weakly entangled states more. As we see in Fig. 1 (c-d), the tails of the histogram for the QJs broaden up (at least for $\Delta S_{\text{qj}} < 0$), indicating that highly entangled states are indeed more fragile and prone to be affected by rare QJs.

To condense the rich information contained in the full statistics of entanglement loss and gain we now focus on the first moment of those distributions, corresponding to the average change to the entanglement entropy due to quantum jumps $\overline{\Delta S_{\text{qj}}}(S, \ell)$ and to the non-Hermitian evolution $\overline{\delta S_{\text{nh}}}(S, \ell)$. We emphasize that these averages [96] depend on S since they are evaluated over the joint distributions $P(\Delta S_{\text{qj}}, S)$ and $P(\delta S_{\text{nh}}, S)$, i.e.

$$\overline{\Delta S_{\text{qj}}}(S, \ell) \equiv \int_{\Delta S_{\text{qj}}} \Delta S_{\text{qj}} P(\Delta S_{\text{qj}}, S) \quad (23)$$

and similarly for $\overline{\delta S_{\text{nh}}}(S, \ell)$. In Fig. 7 (a-b), we plot these first moments for the monitored Ising chain (at a particular point of the phase diagram) for different subsystem sizes ℓ . In panel (a), we see that the change due to non-Hermitian evolution is on average positive, $\overline{\delta S_{\text{nh}}} > 0$, i.e., it induces an *entanglement entropy gain*. This gain is substantial for weakly entangled states, then decreases slowly with the entanglement content. In panel (b), we plot the change due to QJs, normalized with respect to the average waiting time $\bar{\tau}$. As shown in Appendix B, this ratio remains well defined upon increasing the system size L , despite the waiting time vanishing as $\bar{\tau} \sim 1/L$. This is consistent with the idea that a single quantum jump can affect the entanglement entropy of a quantity $O(1/L)$. From Fig. 7(b), we see that $\overline{\Delta S_{\text{qj}}}/\bar{\tau}$ is negative and decreases with S , i.e. QJs on average induce an *entanglement entropy loss*. They do so the more the state onto which they act is entangled. Interestingly, both averages develop a subsystem-size ℓ dependence above a certain threshold entanglement entropy value. A natural question is how these average entanglement gains and losses are connected to the entanglement dynamics under QJs and its phase transition.

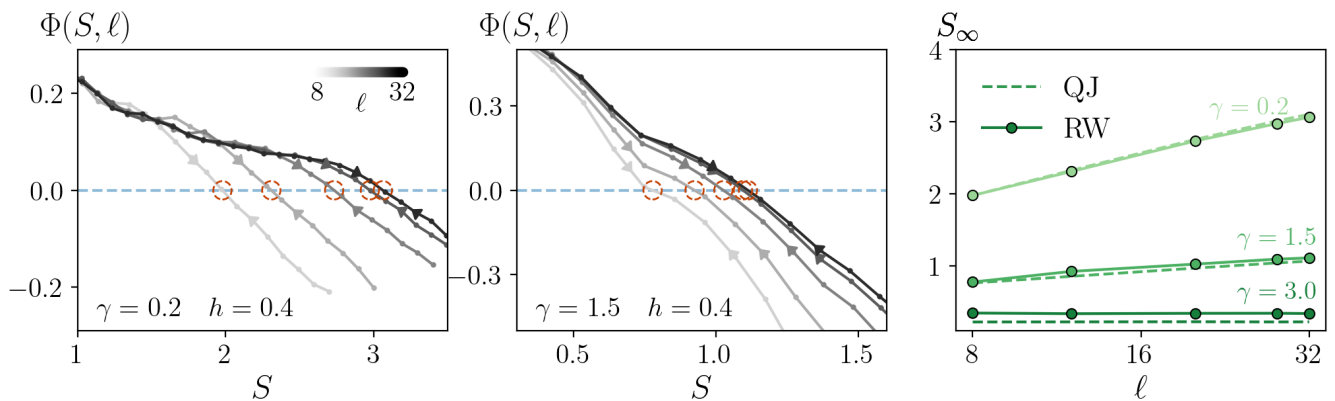


Figure 8: Stochastic model for entanglement dynamics — Panel (a), (b) total rate of entanglement entropy growth obtained, for the monitored Ising chain, from the average entanglement gain and loss, according to Eq. (24). We see the rate $\Phi(S, \ell)$ vanishes at a value $S_\infty(\ell)$ which identifies the steady-state entanglement (circled points). Panel (c) compares S_∞ obtained from the stochastic model with the long-time limit of the entanglement entropy obtained from the full QJ dynamics, showing a perfect agreement.

A. Classical Stochastic Model for Entanglement Dynamics

We now present a classical stochastic model that builds upon the entanglement gain and loss statistics discussed in the previous section and gives a physical picture of the entanglement dynamics under QJs. In particular, we model the entanglement evolution as a random walk with random drift and partial resetting [43, 68, 69], which is sketched in Fig. 1 (e) and that we will now describe. We use the previous analysis showing that the waiting time τ between jumps follows a Poisson law, which means that the random variable can be expressed as $\tau = -\log(r)/(K_\infty(\gamma))$ where $r \in [0, 1]$ is a random number drew for each jump. Then, during this time τ , we model the change of entanglement due to the non-Hermitian evolution by $\Delta S_{\text{nH}} = \tau \delta S_{\text{nH}}$, where δS_{nH} is picked with a probability $P(\delta S_{\text{nH}}, S)$ from the previously computed joint distribution of the effective non-Hermitian slopes. After the time τ , the instantaneous jump happens, and we model the change it has on the entanglement by ΔS_{qj} , which is drawn with a probability $P(\Delta S_{\text{qj}}, S)$ from the corresponding probability distribution. In both cases, the entropy S corresponds to the entanglement before the event (i.e., before the jump or before the non-Hermitian evolution). The probability distributions we use here are taken from the exact sampling of quantum trajectories, binned according to the entanglement entropy content.

The above stochastic process is described by the master equation (1) for the entanglement probability, $P_t(S)$. To understand the role of the first moments of the gain/loss distribution on the entanglement dynamics, it is useful to derive from $P_t(S)$ an equation for the average entanglement entropy, $S = \int dS S P_t(S)$, which reads

$$\frac{dS}{dt} = -\overline{\delta S_{\text{nH}}}(S, \ell) - \overline{\Delta S_{\text{qj}}}(S, \ell)/\bar{\tau} \equiv \Phi(S, \ell) \quad (24)$$

This is a straightforward rate equation for the dynamics of the average entanglement entropy S , which appears to be controlled by a balance between average entanglement gain $\overline{\delta S_{\text{nH}}}(S, \ell)$ and loss $\overline{\Delta S_{\text{qj}}}(S, \ell)$. The fact that these gain/loss rates depend on the value of the entanglement entropy itself, as previously discussed, is crucial here and results in a non-trivial flow of the entanglement entropy with time, encapsulated in the function $\Phi(S, \ell)$ defined in Eq. (24). In Fig. 8 (a-b), we plot $\Phi(S, \ell)$ for the Ising chain (at two particular points of the phase diagram). We see that $\Phi(S, \ell)$ vanishes at a value $S = S_\infty(\ell)$, which by construction identifies the steady-state entanglement and which is obtained when the gain due to non-Hermitian evolution and the loss due to QJs perfectly balance each other, i.e.

$$\Phi(S_\infty, \ell) = \overline{\delta S_{\text{nH}}}(S_\infty, \ell) + \overline{\Delta S_{\text{qj}}}(S_\infty, \ell)/\bar{\tau} = 0. \quad (25)$$

This fixed point is attractive, i.e., depending on the initial condition, it is approached either from the low-entangled branch where $\Phi(S, \ell) > 0$ or from the high-entangled one where $\Phi(S, \ell) < 0$.

We can now validate this stochastic model by extracting the steady-state entanglement S_∞ and its subsystem size ℓ dependence from Eq. (25) for the monitored Ising chain and compare it with the full QJ results discussed in Sec. IV. As shown in Fig. 8(c), the agreement is really good both at weak monitoring, where it reproduces the logarithmic scaling of the entanglement entropy, and in the area law. More importantly, the deal is not limited to the steady-state, but it extends to the full dynamics, as we have shown in Fig. (1) (f). A similar agreement for the steady-state and dynamics of entanglement entropy is also obtained for the monitored SSH model (Appendix D).

We emphasize that the classical stochastic model leading to Eq. (24) is built upon the entanglement gain and loss statistics obtained from the full QJ dynamics. Nev-

ertheless, it still represents a considerable simplification with respect to the total quantum stochastic dynamics, and its agreement points towards the universality of the effect of quantum jump and non-Hermitian evolution on entanglement, which is intriguing and worth exploring further. More importantly, as we will discuss now, it provides a new angle to analyze the dynamics of entanglement under QJs.

VII. STEADY-STATE ENTANGLEMENT BALANCE: NON-HERMITIAN VS JUMPS CONTRIBUTIONS

In this Section, we use the insights from the classical stochastic model to look at the results of the full QJ dynamics presented in Sec. IV from a different perspective. Indeed, we have learned that the steady-state entanglement entropy under QJ monitoring arises from the competition between gain due to the non-Hermitian dynamics and losses due to the jumps. Here, we will discuss the relative balance of these two contributions across the phase diagrams of our two models. This will allow us to shed light on the origin of the entanglement scaling in the two models and the mutual role of jumps and non-Hermitian dynamics. To qualify for a meaningful comparison, we choose values of γ to give the same average waiting time and thus the same number of jumps per trajectory in average.

A. Monitored SSH

Let us start discussing the SSH model at weak monitoring $\gamma = 0.2, h = 1.0$, corresponding to the log-phase discussed in Sec. IV. In Fig 9 (a) we plot separately the average entanglement gain $\overline{\delta S_{\text{nH}}}$ and loss $-\overline{\Delta S_{\text{qj}}}$ (with a minus sign since the steady-state condition from Eq. (25) now reads $\overline{\delta S_{\text{nH}}} = -\overline{\Delta S_{\text{qj}}}/\bar{\tau}$, leading to a crossing between the two rates). We see clearly that the jump contribution depends strongly on subsystem size; the bigger the subsystem, the less QJs decrease the entanglement on average. Interestingly, the subsystem size dependence of this contribution looks logarithmic, as shown in the inset of panel (a). On the other hand, the contribution of the non-Hermitian evolution depends weakly on both ℓ and S , at least for the values of entanglement entropy, which are allowed to be explored by the jumps, i.e., around the crossing point which corresponds to the steady-state entanglement S_{∞} .

This might come as a surprise at first since the bare (no-click) non-Hermitian dynamics would show a clear volume-law scaling for this parameter value. However, unlike the no-click limit, our QJ dynamics reach a steady state when gain and loss are balanced, a condition that is reached for much smaller entanglement entropy. QJs, in other words, confine the non-Hermitian dynamics to small values of entanglement entropy, where it is essen-

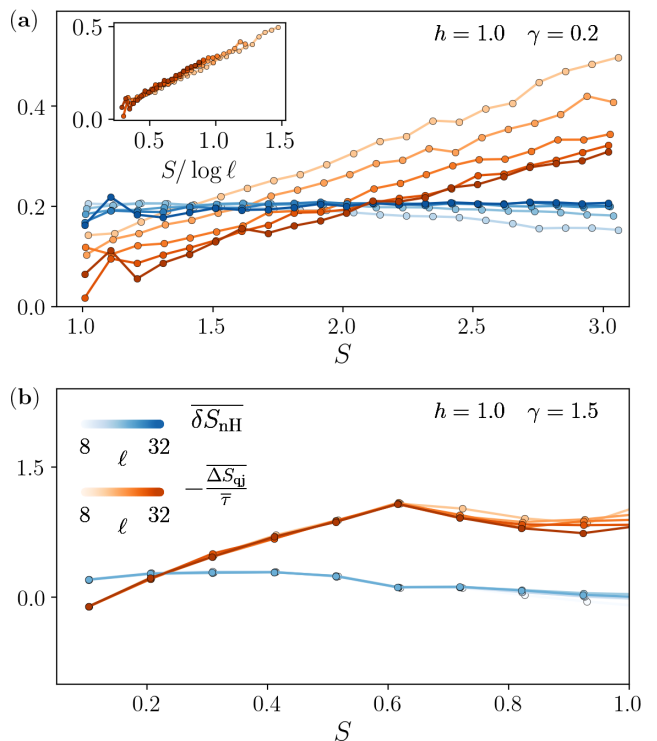


Figure 9: Steady-State Entanglement Balance for the Monitored SSH chain: Average entanglement gain $\overline{\delta S_{\text{nH}}}$ and loss $-\overline{\Delta S_{\text{qj}}}/\bar{\tau}$, as a function of the average entanglement entropy S and different subsystem sizes ℓ (error bars are smaller than the size of the dots). In the weak monitoring phase, Panel (a), the contribution due to QJs scale logarithmically with ℓ (see Inset), while the term arising from the non-Hermitian evolution is practically flat. In the strong monitoring phase, corresponding to the area law, both contributions depend on ℓ . The crossing point corresponds again to the zero of $\Phi(S, \ell)$ i.e., to the steady state entanglement S_{∞} .

tially independent of ℓ . We can, therefore, interpret this result by saying that the effect of QJs here is to *renormalize* the non-Hermitian dynamics into an effective area-law phase. In Appendix C, we discuss the dynamics from a highly entangled state to show how, in that case, one could retrieve a subsystem size dependence in the non-Hermitian contribution, but only at large values of entropy, far above what the system can explore under the effects of QJs.

From this result, we conclude that for the monitored SSH, the logarithmic growth of the entanglement found in Sec. IV arises mainly due to QJs. The picture is that the main effect of increasing the subsystem size is to decrease the slope of ΔS_{qj} , allowing the system to reach a higher value of entanglement entropy. From this point of view, the growth of S should be understood more as a suppression of entanglement loss due to the jumps being less effective in disentangling a large subsystem. In the area law phase (Fig 9 (b)), on the other hand, we see that both contributions are almost independent on ℓ , and

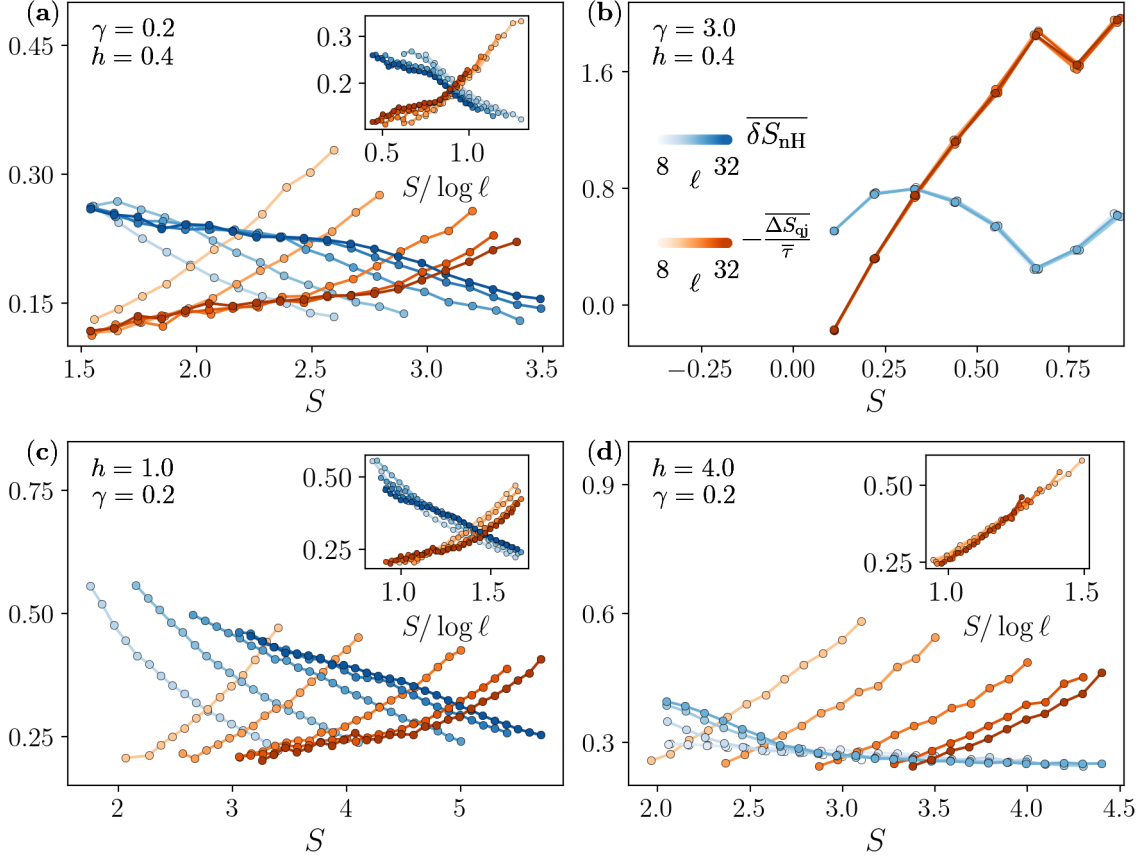


Figure 10: Steady-State Entanglement Balance for the Monitored Ising chain: Average entanglement gain $\overline{\delta S_{\text{nH}}}$ and loss $-\overline{\delta S_{\text{qj}}}/\overline{\tau}$, as a function of the average entanglement entropy S and different subsystem sizes ℓ (error bars are smaller than the size of the dots). In the weak monitoring phase, Panel (a), both contributions scale logarithmically with ℓ (see the inset), suggesting the QJs weakly renormalize the non-Hermitian dynamics. Both terms are independent of subsystem size at strong monitoring (panel b), leading to an area law. Increasing the transverse field (panel c for $h = 1$), the gain contribution due to the non-Hermitian dynamics acquires a non-trivial ℓ dependence (again scaling logarithmically, see inset). Together with the QJ loss term, this leads to a sub-volume steady-state entanglement absent in the no-click limit. For even larger h (panel d, $h = 4$), the non-Hermitian gain term becomes ℓ independent, as in the no-click limit. At the same time, the QJ retains a non-trivial scaling (inset), leading to the observed logarithmic scaling.

their crossing occurs in a regime of small entanglement entropy, leading to an area-law scaling.

B. Monitored Ising Chain

Quite interestingly, the situation is rather different for the Ising chain, as shown in Fig. 10. Let us first consider the weak-monitoring and weak-field regime $\gamma = 0.2$, $h = 0.4$ (panel a), corresponding to the log-phase (see Sec. IV).

As we can see, the entanglement gain $\overline{\delta S_{\text{nH}}}$ and loss $-\overline{\Delta S_{\text{qj}}}/\overline{\tau}$ here show both a non-trivial ℓ dependence, which appears compatible with a logarithmic scaling (see inset). We note that the scaling collapse of our data is expected to occur around the crossing point, indicating the steady-state value S_{∞} . In particular, while the entanglement loss due to QJs behaves similarly to the SSH

case, decreasing with ℓ in absolute value, the entanglement gain due to the renormalized non-Hermitian dynamics, shows a logarithmic scaling with ℓ , as in the no-click limit at this value of parameters. Based on these results, we conclude that in the weak monitoring phase, the non-Hermitian dynamics are only weakly renormalized by QJs. Suppose we increase the monitoring strength $\gamma = 3.0$ (panel b). In that case, the system enters the area law, and we can see that both gain and loss contributions become essentially independent from subsystem size, crossing in a low-entanglement region as expected from an area law.

Let us now consider the region of weak monitoring and large transverse field, where major deviations from the no-click limit were reported (see discussion in Sec. IV). In particular, we fix $\gamma = 0.2$ and scan the transverse field for increasing values of $h > 1$, where the no-click evolution predicts an area-law for the entanglement entropy. At the

same time, the QJ dynamics still showed a logarithmic scaling. In Fig. 10 (c-d), we repeat our analysis of average entanglement gain and loss for different subsystem sizes ℓ . For $h = 1.0$, we again observe strong ℓ dependence in the QJ contribution and the non-Hermitian one. Our steady-state condition (25) predicts a logarithmic scaling for the entanglement entropy, in perfect agreement with the QJ simulation. By breaking down the entanglement content into gain and loss, we can clarify that this log-phase is due to a combined effect of quantum jumps and *renormalised* non-Hermitian evolution.

Finally, upon increasing the transverse field to $h = 4$, we see that the entanglement gain due to the non-Hermitian dynamics becomes essentially ℓ independent, in agreement with the no-click limit. On the other hand, the loss due to QJs scales logarithmically with ℓ (see inset), which results in a steady-state entanglement showing a log-scaling. This logarithmic phase, as for the weak monitoring of the SSH model, is solely due to the QJs. Our analysis therefore highlights two mechanisms at play behind the deviations from the no-click limit observed in the monitored Ising chain phase diagram for $h > 1$. At moderate fields there is a non-trivial renormalization of the non-Hermitian dynamics due to QJs, that leads to a log-scaling of its average gain contribution, as in the weak-monitoring regime of the model. At larger fields instead this renormalisation is washed away, the non-Hermitian dynamics behaves as in the no-click limit and the logarithmic scaling of the entropy arises only from the jumps. While our numerical results does not allow to conclude about the large system size limit, the above analysis suggests that, in absence of a non-trivial non-Hermitian dynamics, the large field log-phase might eventually saturate at large system sizes into an area law, similarly to the weak monitoring phase of the SSH model.

C. Implications for Free Fermions MIPT

Our findings for the average entanglement gain and loss have highlighted the concept of renormalized non-Hermitian dynamics. Due to quantum jumps, which effectively reshuffle the initial state onto which the non-Hermitian Hamiltonian act, the effective non-Hermitian dynamics is renormalized with respect to the bare no-click evolution. We have shown that this renormalization is particularly strong in the weak monitoring phase of the SSH chain, where the jumps wash the no-click volume law entirely away. On the other hand, our results for the Ising chain at weak monitoring points towards a much weaker renormalization. Our results, therefore, highlight a fundamental difference between the weak monitoring phase of the Ising and the SSH chain. While both phases feature a logarithmic scaling of the entanglement entropy, we have demonstrated that the origin of this scaling is very different in the two cases. For the SSH, it comes essentially from the quantum jumps, while for the Ising chain, it is a combined effect of jumps and non-

Hermitian evolution. The same renormalization effect we have shown to be at play in the monitored Ising chain at intermediate and large field values and can, therefore, naturally explain the departure from the no-click limit.

We conclude with a discussion of the implications of our results for the MIPT of free fermions under quantum jumps. The irrelevance of QJs at weak monitoring in the Ising chain is suggestive of a logarithmic phase which could be possibly stable, differently from the SSH case where the jump contributions are likely to saturate at large system sizes through a mechanism similar to the weak-localization correction [33].

VIII. CONCLUSIONS

In this work, we studied the role of quantum jumps on the entanglement dynamics of two models of monitored free fermions, the SSH and Ising chains. In both cases, the no-click limit, corresponding to a deterministic non-Hermitian evolution, was studied in detail and revealed a rich pattern of entanglement transitions. The inclusion of QJ has a somewhat different effect in the two models. On one hand, in the SSH case, the inclusion of jumps qualitatively the physics of the no-click limit, washing away the volume-to-area law transition and leaving a sub-volume phase with logarithmic scaling of entanglement entropy, at least for the system sizes considered in this work. On the other hand, for the Ising chain, our results confirm that the effect of stochastic jumps is mainly quantitative, except in specific areas of the phase diagram where deviations from the no-click limit appear.

To better understand the origin of such a different impact of QJs, we have first computed their statistics, particularly their waiting-time distribution. Surprisingly, we have found that at long times, both models acquire a universal Poisson distribution of waiting times, with the same average waiting time $\bar{\tau}$. Then, we introduced an unexplored characterization based on the entanglement gain and loss statistics after or between quantum jumps. The resulting histogram display, particularly for the quantum jump case, has a very broad distribution and a typical value pinned close to zero, suggesting that most QJs are not significantly affecting the entanglement controlled by rare jump events.

Using the full statistics of entanglement gain and loss, we have built a stochastic random walk model with partial resetting, which can reproduce the full QJ dynamics of entanglement entropy for both models. This model offers a new light for interpreting the QJ numerics. Indeed, it suggests a natural steady-state condition for the entanglement entropy, given by the balance between gain due to the non-Hermitian evolution and losses due to quantum jumps. Remarkably, this condition accurately reproduced the scaling of entanglement entropy with subsystem size obtained by the full QJ dynamics. Furthermore, it clarified the origin of the different entanglement scaling and the mutual role of jumps and non-Hermitian

evolution.

The outcome of this analysis reveals a compelling difference between the two models. Indeed, while for the SSH, the sub-volume phase at weak-monitoring is mainly due to the jumps, which allows larger and larger values of entanglement entropy to be accessed, leading to an overall growth with ℓ , for the Ising chain, the weak-monitoring phase arises from the interplay of jumps becoming less effective in destroying entanglement and non-Hermitian evolution creating more and more entanglement. Furthermore, our analysis allows us to identify the source of the unexpected logarithmic scaling of the entanglement in the monitored Ising chain at large fields due to the renormalized non-Hermitian evolution dressed by quantum jumps.

An interesting future direction could be to use the statistics of entanglement gain and loss introduced here to study non-integrable, interacting monitored quantum systems under quantum jumps [24]. Here one can expect the volume law phase to be stable, at least up to a critical monitoring rate. One could therefore expect a different statistics of entanglement loss in this case, reflecting the differences in how gaussian and genuine ergodic quantum states respond to quantum measurements.

Acknowledgments

We thank A. Biella, M. Buchhold, J. Dalibard, M. Dalmonte, R. Fazio, A. Pavigianiti, L. Piroli, A. Romito, P. Sierant, and A. Silva for discussions and collaborations on related topics. We acknowledge computational resources on the Collège de France IPH cluster. X.T. acknowledge DFG under Germany's Excellence Strategy – Cluster of Excellence Matter and Light for Quantum Computing (ML4Q) EXC 2004/1 – 390534769, and DFG Collaborative Research Center (CRC) 183 Project No. 277101999 - project B01.

Note added. During the completion of this work, we become aware of a related manuscript by C. Leung, et al. appearing in the same arXiv posting, studying the stability of the non-Hermitian Hamiltonian for quantum state diffusion [93].

Appendix A: Statistics of the monitored observable

A different perspective on the role of quantum jumps in the monitored dynamics of our two models can be obtained by looking at the statistics of the monitored observable, in this case, the histogram of the local density. As discussed in Sec. III, this provides information that is not contained in the average dynamics described by the Lindbladian, which only captures the average value (first moment) of the histogram.

To appreciate this point in Fig. 11, we plot for the monitored SSH the statistics of the particle density in the A sublattice for increasing values of the monitoring rate

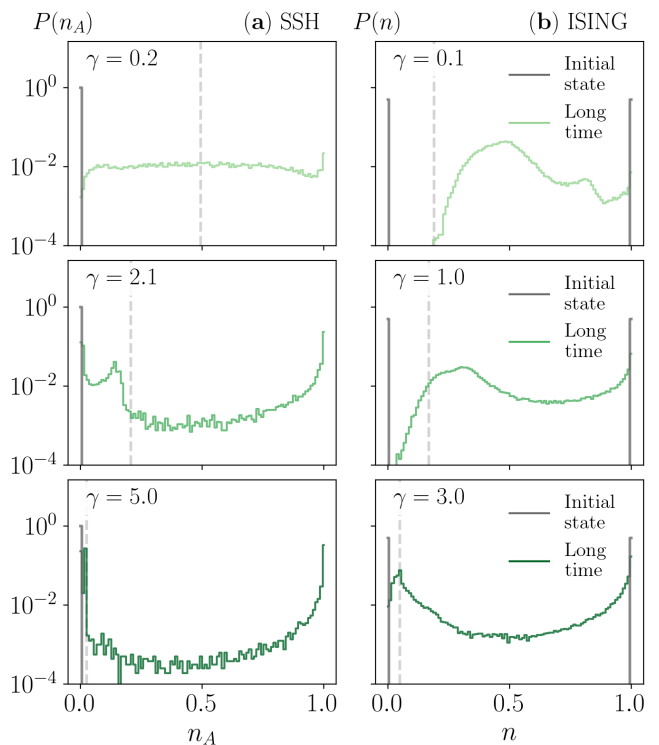


Figure 11: Statistics of the particle density for the SSH (left panels), corresponding to the sublattice A , and for the Ising chain (right panels). Upon increasing the monitoring rate we see the emergence of a strong bimodality, with one of the two peaks that appear in correspondence of the non-Hermitian evolution result.

γ . Given the choice of our initial state, this histogram at time $t = 0$ is peaked at $n_A = 0$, but at long times, we see a redistribution due to the interplay of non-Hermitian dynamics and jumps. For weak monitoring, we see that the long-time limit is an almost flat distribution where all measurement outcomes are almost equally probable, except for the region near $n_A = 1$, which features a small peak reminiscent of the fact that jumps in the SSH model gets rid of state with empty sites in the A sublattice. For comparison, we show the average density predicted by the non-Hermitian evolution as a dashed line.

As the monitoring strength increases, we see that the most likely outcome is always $n_A = 1$. However, there is a secondary peak that appears near $n_A = 0$. For strong monitoring, when the system is in the area of law, this secondary peak is very close to the value predicted by the non-Hermitian Hamiltonian. This analysis confirms, therefore, that, at large monitoring, the influence of the non-Hermitian evolution is present in the full QJ dynamics. It also explains that the entanglement entropy shows an area law scaling in both cases since the long-time steady-state limit at large γ are two CDW states that only have $O(1)$ entanglement.

In the right panels of Fig. 11, we plot the particle density (or local transverse magnetization) statistics for the

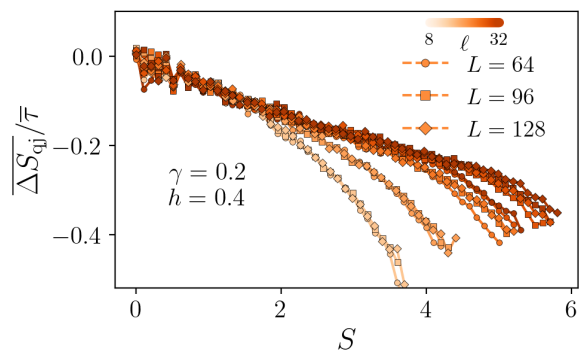


Figure 12: Loss distribution $\Delta S_{\text{qj}}/\bar{\tau}$ obtained in the Ising model for different system sizes $L = 64, 96, 128$. The distribution is invariant regarding the system size; we observe a slight disagreement at large subsystem sizes ℓ in the small system $L = 64$, which is due to the finite size effect.

Ising chain. Here, we see a different behavior at weak monitoring; a gap appears in the histogram of particle density in correspondence with the values $n = 0$, which is gradually filled with increasing γ . As the monitoring rate is further increased, a bimodal structure emerges, as already observed in Ref. [52], in correspondence with the value expected from the non-Hermitian dynamics (dashed line).

We emphasize that to appreciate this point, we need to look at the full histogram of particle density since the average value described by the Lindblad master equation only illustrates that the system wants to reach a uniform steady state.

Appendix B: System size scaling of entanglement loss

In the main text we introduced a classical stochastic model for the entanglement entropy dynamics, which builds upon the entanglement gain and loss statistics. In particular, the role of QJs is to induce an entanglement loss that, in the stationary state, is balanced by the gain provided by the non-Hermitian evolution, as described in Eq. (24) of the main text. This equation divides the entanglement loss by the average waiting time $\bar{\tau}$, which considers the instantaneous nature of QJs. As we have seen in Sec. V, the average waiting time scales as $1/L$, which raises the question of the stability of the steady-state condition in the large system size limit. In this Appendix, we provide evidence supporting the statement that the average entanglement loss due to the jump scales as $1/L$, so the ratio with the averaging waiting time remains finite when $L \rightarrow \infty$. In Fig. 12, we plot, for the monitored Ising chain at a representative value of the parameters, the average entanglement loss divided by the waiting time, $\overline{\Delta S_{\text{qj}}}(S, \ell)/\bar{\tau}$ as a function of S, ℓ and different system sizes. We see that the data corresponding to different sizes collapsing onto each other for each sub-

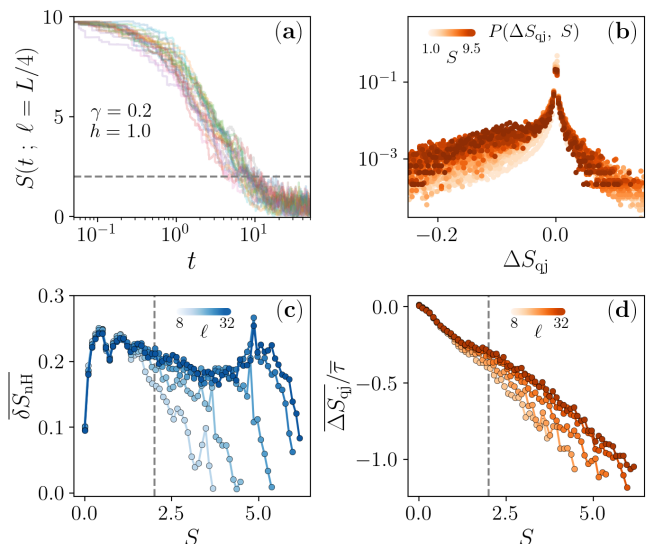


Figure 13: Analysis of trajectories obtained from a highly entangled initial state in the SSH model. Panel (a) : Entanglement Dynamics in the monitored SSH chain under QJ dynamics with an initial state highly entangled (namely a steady state of the no-click limit). Panel (b) : Conditioned version of the distribution ΔS_{qj} with respect to the entanglement when the jumps is happening. Panel (c) : First moment of the conditioned distribution ΔS_{qj} and δS_{NH} in function of the entanglement S_e obtained with these trajectories

system sizes ℓ , which demonstrate this invariance of the ratio $\overline{\Delta S_{\text{qj}}}/\bar{\tau}$.

Appendix C: Quantum jumps from highly entangled initial states

In this Appendix we provide evidence to support the conjecture that highly entangled states are more fragile to measurements than weakly entangled ones. To this extent, we consider the monitored SSH chain starting from an initial condition corresponding to the long-time limit of the associated non-Hermitian Hamiltonian, which is known to support volume-law entangled states for small values of γ . In Fig. 13 (a) we show a sample of trajectories for the entanglement entropy, all converging towards a steady-state value with low entanglement (and equal to the steady-state reached from a product state initial condition). In other words, the system under monitoring cannot sustain volume-law entanglement. In panel (b) we plot the joint distribution of entanglement loss $P(\Delta S_{\text{qj}}, S)$, which now displays a broadening of its tails indicating that the role of jumps become more relevant. In particular we see that the probability of a large entanglement loss due to atypical jumps increases, which explains why high entanglement cannot be preserved. In panels (c-d) we present the same analysis given in the main text on the first moments of the gain/loss joint distributions, $\overline{\Delta S_{\text{qj}}}, \overline{\delta S_{\text{NH}}}$, but for this particular initial con-

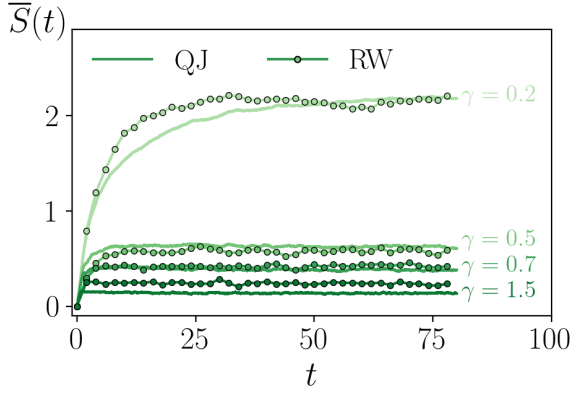


Figure 14: Entanglement dynamics as a classical random walk for the SSH model — Comparison between the dynamics of the average entanglement entropy obtained from the exact quantum jump dynamics (QJ) or the phenomenological classical random walk (RW).

dition. We note that in the region of low entanglement, for $S \leq 2$ (see dashed line) which contains the steady-state (see panel a), the average entanglement gain from non-Hermitian dynamics is essentially independent from subsystem size ℓ , a behavior similar to what observed in Fig. 9 for a different initial condition. However, as the system dynamics explores larger values of entanglement entropy ($S \geq 2$) throughout its evolution we see important subsystem size effects in $\delta\bar{S}_{\text{nH}}$, which would be hidden otherwise starting from a low entangled initial condition.

Appendix D: Stochastic model for the SSH setup

In this Appendix we present the results obtained for the monitored SSH model using the classical random-walk with resetting for entanglement dynamics. To obtain these results we proceed as discussed in the main text and summarized in Fig. 1, namely we first compute numerically the joint gain/loss probabilities $P(\delta S_{\text{nH}}, S)$, $P(\Delta S_{\text{qj}}, S)$ and then we feed them into the classical master equation to build the associated stochastic process. In Fig. 14 we plot the dynamics of the average entanglement entropy obtained from the random walk (RW) with drift and resetting and compare it with the exact numerical results of the quantum trajectories. As for the monitored Ising chain discussed in Sec. II, the agreement is excellent for both weak and strong monitoring rates γ , confirming that the classical model is able to capture the entanglement transition also in the monitored SSH chain.

Appendix E: Free Fermion Techniques with Quantum Jumps

This Section provides details on solving the stochastic Schrödinger dynamics using free-fermion techniques. Since the Hamiltonian we consider for both models is quadratic, and the monitoring process preserves Gaussianity, the state $|\psi\rangle$ is entirely determined by the 2-point correlation matrix C thanks to Wick's theorem. We can either store the state in this correlation matrix or use another representation that uses the fact that we consider pure states.

1. Correlation matrix

In general, to solve the Schrödinger equation in a free fermions problem, we use Wick's theorem to rewrite the equation in terms of the correlation matrix

$$C(t) = \begin{pmatrix} G(t) & F(t) \\ F(t)^\dagger & 1 - G(t)^T \end{pmatrix} \quad (\text{E1})$$

where $C_{m,n}(t) = \langle \Psi(t) | \mathbf{c}_m^\dagger \mathbf{c}_n | \Psi(t) \rangle$ is a matrix of size $2L \times 2L$ and $\mathbf{c}^T = (c_1 \ c_2 \ \dots \ c_L \ c_1^\dagger \ c_2^\dagger \ \dots \ c_L^\dagger)$. We get for the deterministic part when measuring the local density, the equation [43]

$$\frac{dC(t)}{dt} = 2i[\mathbb{H}, C(t)] + \gamma C \Lambda C - \gamma \Lambda_+ C \Lambda_+ + \gamma \Lambda_- C \Lambda_- \quad (\text{E2})$$

where $\Lambda_+ = \mathbb{1}_L \otimes (\sigma_z + 1)/2$, $\Lambda_- = \mathbb{1}_{2L} - \Lambda_+$ and $\Lambda = \mathbb{1}_L \otimes \sigma_z$, $\sigma_z = \text{diag}(1, -1)$ is the Pauli matrix and \mathbb{H} is defined such that $H = \mathbf{c}^\dagger \mathbb{H} \mathbf{c}$.

The von Neumann entanglement of a subsystem of size ℓ can be extracted through the Majorana fermions correlation matrix [43, 94]. Effectively we get it by diagonalizing the following matrix

$$\mathcal{A}(t) = \begin{pmatrix} \mathcal{G}_\ell^I + \mathcal{F}_\ell^I & \mathcal{G}_\ell^R - \mathcal{F}_\ell^R - \mathbb{1} \\ \mathbb{1} - \mathcal{G}_\ell^R - \mathcal{F}_\ell^R & \mathcal{G}_\ell^I + \mathcal{F}_\ell^I \end{pmatrix} \quad (\text{E3})$$

with $2\mathcal{G}_{\ell \times \ell}^R = \mathcal{G}_\ell^R + i\mathcal{G}_\ell^I$ and $2\mathcal{F}_{\ell \times \ell}^R = \mathcal{F}_\ell^R + i\mathcal{F}_\ell^I$, which has an imaginary spectrum. The entanglement is given by the formula

$$S_A(t) = - \sum_{j=1}^{\ell} \nu_j(t) \ln[\nu_j(t)] + (1 - \nu_j(t)) \ln[1 - \nu_j(t)] \quad (\text{E4})$$

with $\nu_j(t) = (1 - \lambda_j(t))/2$ where $\lambda_j(t)$ are the ℓ eigenvalues of $\mathcal{A}(t)$ with a positive imaginary part.

Jumps such that $L_j \propto n_j$ (i.e., we measure the local density) can be implemented at the level of the correlation matrix. For a jump on site l we have

$$dF_{m,n}^J = \begin{cases} 1, & \text{if } n = m = l \\ 0, & \text{if } m = l, n \neq l \text{ or } m \neq l, n = l \\ G_{m,n} - \frac{G_{m,l}G_{l,n} + F_{m,l}(F^\dagger)_{n,l}}{G_{l,l}}, & \text{otherwise} \end{cases} \\ dF_{m,n} = \frac{G_{n,l}F_{l,m} + G_{m,l}F_{l,n}}{G_{l,l}}. \quad (\text{E5})$$

To avoid numerical instabilities, it is advisable to explicitly write the zeros in the matrix update.

In the algorithm used in this work, the goal is to find the time at which the jump happens, thus we need to be able to evaluate the decay of the norm during the non-Hermitian evolution to find this time. To do so, we solve numerically the equation

$$\frac{d}{dt}\langle\tilde{\Psi}(t)|\tilde{\Psi}(t)\rangle = -\gamma\langle\tilde{\Psi}(t)|\tilde{\Psi}(t)\rangle \sum_j G_{j,j}(t) \quad (\text{E6})$$

where $G_{j,j}(t)$ is obtain by solving the correlation matrix equation of motion in parallel and $|\tilde{\Psi}(t)\rangle$ is the unnormalized wavefunction. Then we can find by bisection for each jump the time at which it happens [71].

When the model presents a $U(1)$ symmetry it is simpler because the conservation of the number of particles reduces by a factor of 2 the size of the correlation matrix to consider. Indeed, we have to consider only the matrix $G_{m,n}(t) = \langle\psi(t)|\mathbf{c}_m^\dagger\mathbf{c}_n|\psi(t)\rangle$ with $\mathbf{c}^T = (c_1 c_2 \dots c_L)$. Here we gives the equation that can be used for the SSH model and for convenience we will use a basis respecting the site A and B of the model, thus we consider the basis where $c_{2k-1} = c_{A,k}$ and $c_{2k} = c_{B,k}$ for $1 \leq k \leq L/2$. In that case we get for the deterministic part (when measuring $n_{A,i}$ and $1 - n_{B,i}$), the equation [43]

$$\frac{dG(t)}{dt} = 2i[\mathbb{H}, G(t)] + \gamma G \Lambda_G - \gamma \Lambda_A C \Lambda_A + \gamma \Lambda_B G \Lambda_B \quad (\text{E7})$$

where $\Lambda_A = \mathbb{1}_{L/2} \otimes (\sigma_z + 1)/2$, $\Lambda_B = \mathbb{1}_L - \Lambda_A$ and $\Lambda = \mathbb{1}_{L/2} \otimes \sigma_z$ and \mathbb{H} defined such that $H = \mathbf{c}^\dagger \mathbb{H} \mathbf{c}$. Then the other methods to do the jumps apply directly.

2. Wavefunction representation

When the system conserves the number of particles, as in the monitored SSH case, not only the correlation matrix approach described above simplifies but one can also use a different approach based on representing the wavefunction as

$$|\psi(t)\rangle = P(t)c_{i_1}^\dagger \dots c_{i_N}^\dagger |0\rangle = \prod_{k=1}^N \sum_{m=1}^L U_{m,k}(t)c_m^\dagger |0\rangle \quad (\text{E8})$$

where we consider N particles. Then the $U(t)$ matrix can be updated through $\tilde{U}(t+dt) = e^{-i\mathbb{H}_{\text{eff}}dt}U(t)$ [29]. Nonetheless, when H_{eff} is non Hermitian, the state should be normalised. This is done by performing a QR decomposition on $\tilde{U}(t+dt)$, which normalize the state without modifying it. The correlation matrix $G(t)$ is then obtained through

$$G(t) = U(t)^*U(t)^T \quad \text{with} \quad \tilde{U}(t) = U(t)R(t). \quad (\text{E9})$$

We can implement the jumps as previously at the level of this correlation matrix like in Eq. E5. In the case of

the SSH model we are also considering jumps of the form $L_j \propto 1 - n_j$ in that case the update of $G(t)$ is such that

$$G_{m,n}^J = \begin{cases} 0, & \text{if } n = m = l \\ 0, & \text{if } m = l, n \neq l \text{ or } m \neq l, n = l \\ G_{m,n} + \frac{G_{m,l}G_{l,n}}{1-G_{l,l}}, & \text{otherwise.} \end{cases}$$

The jumps preserve the gaussianity and $U(1)$ symmetry, thus the new correlation matrix is of the form $G(t) = U(t)^*U(t)^T$ thus is semi-definite positive hermitian, and the k^{th} vector column of $U(t)$ called U_k satisfy

$$G(t)U_k^* = U_k^* \quad 1 \leq k \leq N. \quad (\text{E10})$$

Then the SVD decomposition $G(t) = U_{\text{SVD}}DU_{\text{SVD}}^\dagger$ gives directly these eigenvectors, and the restriction of the first N columns with eigenvalue 1 (i.e. the N particles) gives

$$U(t) = (U_{\text{SVD}})_{L \times N}. \quad (\text{E11})$$

Since the columns of U_{SVD} are orthogonal the state is well normalized and correctly defined. Like in the previous subsection we need the decay of the norm to evaluate the time at which the jump is happening. In that case, the norm can be directly obtained from the QR decomposition, indeed

$$\langle\tilde{\Psi}(t)|\tilde{\Psi}(t)\rangle = \prod_{j=1}^N R(t)_{j,j}R(t)_{j,j}^*, \quad (\text{E12})$$

where $R(t)$ is the matrix from Eq. E9.

This kind of representation of the wavefunction can be extended to the general case without particle number conservation. In that case we have that [95]

$$|\psi(t)\rangle = \mathcal{N} \exp\left(-\frac{1}{2} \sum_{i,j} [(U(t)^\dagger)^{-1}V(t)^\dagger]_{i,j} c_i^\dagger c_j^\dagger\right) |0\rangle \quad (\text{E13})$$

where \mathcal{N} enforces the normalization, and the evolution is given by imposing that $\gamma_k(t)|\psi(t)\rangle = 0$ with $\gamma_k(t) = \sum_j V_{j,k}^*(t)c_j^\dagger + U_{j,k}^*(t)c_j$. And we now evolve the 2 matrices $U(t)$ and $V(t)$ through

$$\begin{pmatrix} U(t) \\ V(t) \end{pmatrix} = e^{-2i\mathbb{H}_{\text{eff}}t} \begin{pmatrix} U(0) \\ V(0) \end{pmatrix}. \quad (\text{E14})$$

Since the evolution is non Hermitian the state is here again not normalized, but this can be enforce through the factor \mathcal{N} . As significantly, to guaranty that $\gamma_k(t)$ is a well define fermionic operator we have to impose

$$\begin{cases} U(t)^\dagger U(t) + V(t)^\dagger V(t) = \mathbb{1} \\ V^T(t)U(t) + U^T(t)V(t) = 0 \end{cases} \quad (\text{E15})$$

This can be done by performing a QR decomposition on

$$\mathbb{U}(t) = \begin{pmatrix} U(t) & V(t)^* \\ V(t) & U(t)^* \end{pmatrix} \quad (\text{E16})$$

as proved in Ref. [35] To implement the jump within this framework, we can compute the correlation matrix $C(t)$ which is given by

$$C(t) = \begin{pmatrix} U(t)U(t)^\dagger & U(t)V^\dagger(t) \\ V(t)U^\dagger(t) & V(t)V^\dagger(t) \end{pmatrix} \quad (\text{E17})$$

As in the $U(1)$ case, we then need to retrieve the state matrix, which is done using a SVD decomposition of the correlation matrix.

-
- [1] P. Calabrese and J. Cardy, *Journal of Statistical Mechanics: Theory and Experiment* **2005**, P04010 (2005).
- [2] H. Liu and S. J. Suh, *Phys. Rev. Lett.* **112**, 011601 (2014).
- [3] A. Nahum, J. Ruhman, S. Vijay, and J. Haah, *Phys. Rev. X* **7**, 031016 (2017).
- [4] G. D. Chiara, S. Montangero, P. Calabrese, and R. Fazio, *Journal of Statistical Mechanics: Theory and Experiment* **2006**, P03001 (2006).
- [5] H. Kim and D. A. Huse, *Phys. Rev. Lett.* **111**, 127205 (2013).
- [6] J. H. Bardarson, F. Pollmann, and J. E. Moore, *Phys. Rev. Lett.* **109**, 017202 (2012).
- [7] M. P. Fisher, V. Khemani, A. Nahum, and S. Vijay, *Annu. Rev. Condens. Matter Phys.* **14**, 335 (2023).
- [8] A. C. Potter and R. Vasseur, *Quantum Sciences and Technology* (Springer, Cham, 2022) p. 211.
- [9] O. Lunt, J. Richter, and A. Pal, *Quantum Sciences and Technology* (Springer, Cham, 2022) p. 251.
- [10] M. J. Gullans and D. A. Huse, *Phys. Rev. X* **10**, 041020 (2020).
- [11] C. Noel, P. Niroula, D. Zhu, A. Risinger, L. Egan, D. Biswas, M. Cetina, A. V. Gorshkov, M. J. Gullans, D. A. Huse, and C. Monroe, *Nature Phys.* **18**, 760 (2022).
- [12] J. M. Koh, S.-N. Sun, M. Motta, and A. J. Minnich, *Nature Phys.* **19**, 1314 (2023).
- [13] Google AI and Collaborators, *Nature* **622**, 481–486 (2023).
- [14] Y. Li, X. Chen, and M. P. A. Fisher, *Phys. Rev. B* **98**, 205136 (2018).
- [15] Y. Li, X. Chen, and M. P. A. Fisher, *Phys. Rev. B* **100**, 134306 (2019).
- [16] B. Skinner, J. Ruhman, and A. Nahum, *Phys. Rev. X* **9**, 031009 (2019).
- [17] M. Szyniszewski, A. Romito, and H. Schomerus, *Phys. Rev. B* **100**, 064204 (2019).
- [18] C.-M. Jian, Y.-Z. You, R. Vasseur, and A. W. W. Ludwig, *Phys. Rev. B* **101**, 104302 (2020).
- [19] S. Choi, Y. Bao, X.-L. Qi, and E. Altman, *Phys. Rev. Lett.* **125**, 030505 (2020).
- [20] A. Zabalo, M. J. Gullans, J. H. Wilson, R. Vasseur, A. W. W. Ludwig, S. Gopalakrishnan, D. A. Huse, and J. H. Pixley, *Phys. Rev. Lett.* **128**, 050602 (2022).
- [21] P. Sierant and X. Turkeshi, *Phys. Rev. Lett.* **128**, 130605 (2022).
- [22] P. Sierant, M. Schirò, M. Lewenstein, and X. Turkeshi, *Phys. Rev. B* **106**, 214316 (2022).
- [23] K. Klocke and M. Buchhold, *Phys. Rev. X* **13**, 041028 (2023).
- [24] Y. Fuji and Y. Ashida, *Phys. Rev. B* **102**, 054302 (2020).
- [25] O. Lunt and A. Pal, *Phys. Rev. Res.* **2**, 043072 (2020).
- [26] E. V. H. Doggen, Y. Gefen, I. V. Gornyi, A. D. Mirlin, and D. G. Polyakov, *Phys. Rev. Res.* **4**, 023146 (2022).
- [27] B. Xing, X. Turkeshi, M. Schirò, R. Fazio, and D. Poletti, (2023), [arXiv:2308.09133 \[quant-ph\]](https://arxiv.org/abs/2308.09133) .
- [28] A. Altland, M. Buchhold, S. Diehl, and T. Micklitz, *Phys. Rev. Res.* **4**, L022066 (2022).
- [29] X. Cao, A. Tilloy, and A. De Luca, *SciPost Phys.* **7**, 024 (2019).
- [30] L. Fidkowski, J. Haah, and M. B. Hastings, *Quantum* **5**, 382 (2021).
- [31] M. Coppola, E. Tirrito, D. Karevski, and M. Collura, *Phys. Rev. B* **105**, 094303 (2022).
- [32] H. Lóio, A. De Luca, J. De Nardis, and X. Turkeshi, *Phys. Rev. B* **108** (2023).
- [33] I. Poboiko, P. Pöpperl, I. V. Gornyi, and A. D. Mirlin, *Phys. Rev. X* **13**, 041046 (2023).
- [34] C.-M. Jian, H. Shapourian, B. Bauer, and A. W. W. Ludwig, (2023), [arXiv:2302.09094](https://arxiv.org/abs/2302.09094) .
- [35] M. Fava, L. Piroli, T. Swann, D. Bernard, and A. Nahum, *Phys. Rev. X* **13**, 041045 (2023).
- [36] C. Carisch, A. Romito, and O. Zilberberg, (2023), [arXiv:2304.02965 \[quant-ph\]](https://arxiv.org/abs/2304.02965) .
- [37] T. Jin and D. G. Martin, (2023), [arXiv:2309.15034 \[quant-ph\]](https://arxiv.org/abs/2309.15034) .
- [38] O. Alberton, M. Buchhold, and S. Diehl, *Phys. Rev. Lett.* **126**, 170602 (2021).
- [39] M. Van Regemortel, Z.-P. Cian, A. Seif, H. Dehghani, and M. Hafezi, *Phys. Rev. B* **126** (2021).
- [40] X. Turkeshi, A. Biella, R. Fazio, M. Dalmonte, and M. Schirò, *Phys. Rev. B* **103**, 224210 (2021).
- [41] T. Botzung, S. Diehl, and M. Müller, *Phys. Rev. B* **104**, 184422 (2021).
- [42] Y. Bao, S. Choi, and E. Altman, *Ann. Phys.* **435**, 168618 (2021).
- [43] X. Turkeshi, M. Dalmonte, R. Fazio, and M. Schirò, *Phys. Rev. B* **105**, L241114 (2022).
- [44] G. Piccitto, A. Russomanno, and D. Rossini, *Phys. Rev. B* **105**, 064305 (2022).
- [45] G. Kells, D. Meidan, and A. Romito, *SciPost Phys.* **14**, 031 (2023).
- [46] A. Paviglianiti and A. Silva, *Phys. Rev. B* **108**, 184302 (2023).
- [47] T. Müller, S. Diehl, and M. Buchhold, *Phys. Rev. Lett.* **128**, 010605 (2022).
- [48] M. Buchhold, T. Müller, and S. Diehl, (2022), [arXiv:2208.10506 \[cond-mat.dis-nn\]](https://arxiv.org/abs/2208.10506) .
- [49] J. Dalibard, Y. Castin, and K. Mølmer, *Phys. Rev. Lett.* **68**, 580 (1992).
- [50] M. B. Plenio and P. L. Knight, *Rev. Mod. Phys.* **70**, 101 (1998).
- [51] H. M. Wiseman and G. J. Milburn, *Quantum Measurement and Control* (Cambridge University Press, Cambridge, England, 2009).
- [52] A. Biella and M. Schirò, *Quantum* **5**, 528 (2021).
- [53] S. Gopalakrishnan and M. J. Gullans, *Phys. Rev. Lett.*

- 126**, 170503 (2021).
- [54] S.-K. Jian, Z.-C. Yang, Z. Bi, and X. Chen, *Phys. Rev. B* **104**, L161107 (2021).
- [55] X. Turkeshi and M. Schiró, *Phys. Rev. B* **107**, L020403 (2023).
- [56] Y. L. Gal, X. Turkeshi, and M. Schiró, *SciPost Phys.* **14**, 138 (2023).
- [57] K. Kawabata, T. Numasawa, and S. Ryu, *Phys. Rev. X* **13**, 021007 (2023).
- [58] T. Orito and K.-I. Imura, *Phys. Rev. B* **108**, 214308 (2023).
- [59] C. Zerba and A. Silva, *SciPost Phys. Core* **6**, 051 (2023).
- [60] E. Granet, C. Zhang, and H. Dreyer, *Phys. Rev. Lett.* **130**, 230401 (2023).
- [61] L. Su, A. Clerk, and I. Martin, (2023), [arXiv:2306.07428 \[quant-ph\]](#) .
- [62] T. Banerjee and K. Sengupta, (2023), [arXiv:2309.07661 \[cond-mat.str-el\]](#) .
- [63] G. Lee, T. Jin, Y.-X. Wang, A. McDonald, and A. Clerk, (2023), [arXiv:2308.14614 \[quant-ph\]](#) .
- [64] F. Minganti, A. Miranowicz, R. W. Chhajlany, and F. Nori, *Phys. Rev. A* **100**, 062131 (2019).
- [65] C. Gneiting, A. V. Rozhkov, and F. Nori, *Phys. Rev. A* **104**, 062212 (2021).
- [66] M. Naghiloo, M. Abbasi, Y. N. Joglekar, and K. W. Murch, *Nature Physics* **15**, 1232 (2019).
- [67] P. Han, F. Wu, X. Huang, H. Wu, C.-L. Zou, W. Yi, M. Zhang, H. Li, K. Xu, D. Zheng, H. Fan, J. Wen, Z. Yang, and S. Zheng, (2023), [arXiv:2210.04494 \[quant-ph\]](#) .
- [68] M. R. Evans and S. N. Majumdar, *Phys. Rev. Lett.* **106**, 160601 (2011).
- [69] M. R. Evans, S. N. Majumdar, and G. Schehr, *J. Phys. A: Math. Theor.* **53**, 193001 (2020).
- [70] H.-P. Breuer and F. Petruccione, *The Theory of Open Quantum Systems* (Oxford University Press, Oxford, England, 2002).
- [71] A. J. Daley, *Adv. Phys.* **63**, 77 (2014).
- [72] C. Cohen-Tannoudji and J. Dalibard, *Europhysics Letters* **1**, 441 (1986).
- [73] G. T. Landi, M. J. Kewming, M. T. Mitchison, and P. P. Potts, (2023), [arXiv:2303.04270 \[quant-ph\]](#) .
- [74] P. Calabrese and J. Cardy, *J. Stat. Mech.* **2004**, P06002 (2004).
- [75] L. Amico, R. Fazio, A. Osterloh, and V. Vedral, *Rev. Mod. Phys.* **80**, 517 (2008).
- [76] E. Tirrito, A. Santini, R. Fazio, and M. Collura, *SciPost Phys.* **15**, 096 (2023).
- [77] X. Turkeshi, L. Piroli, and M. Schiró, (2023), [arXiv:2306.09893 \[cond-mat.stat-mech\]](#) .
- [78] J. Ferreira, T. Jin, J. Mannhart, T. Giamarchi, and M. Filippone, (2023), [arXiv:2306.16452 \[quant-ph\]](#) .
- [79] X. Turkeshi, L. Piroli, and M. Schiró, *Phys. Rev. B* **106**, 024304 (2022).
- [80] M. Buchhold, Y. Minoguchi, A. Altland, and S. Diehl, *Phys. Rev. X* **11**, 041004 (2021).
- [81] I. Poboiko, I. V. Gornyi, and A. D. Mirlin, (2023), [arXiv:2309.12405 \[quant-ph\]](#) .
- [82] K. Chahine and M. Buchhold, (2023), [arXiv:2309.12391 \[cond-mat.str-el\]](#) .
- [83] A. Paviglianiti, X. Turkeshi, M. Schiró, and A. Silva, (2023), [arXiv:2310.02686 \[quant-ph\]](#) .
- [84] S. Murciano, P. Sala, Y. Liu, R. S. K. Mong, and J. Alicea, *Phys. Rev. X* **13**, 041042 (2023).
- [85] H. J. Carmichael, S. Singh, R. Vyas, and P. R. Rice, *Phys. Rev. A* **39**, 1200 (1989).
- [86] A. Delteil, W.-b. Gao, P. Fallahi, J. Miguel-Sanchez, and A. Imamoğlu, *Phys. Rev. Lett.* **112**, 116802 (2014).
- [87] T. Brandes, *AIP Conference Proceedings* **1074**, 102 (2008).
- [88] M. Albert, G. Haack, C. Flindt, and M. Büttiker, *Phys. Rev. Lett.* **108**, 186806 (2012).
- [89] G. T. Landi, *Phys. Rev. B* **104**, 195408 (2021).
- [90] G. T. Landi, (2023), [arXiv:2305.07957 \[quant-ph\]](#) .
- [91] M. Coppola, D. Karevski, and G. T. Landi, Conditional no-jump dynamics of non-interacting quantum chains (2023), [arXiv:2311.05515 \[cond-mat.stat-mech\]](#) .
- [92] F. Bardou, J. P. Bouchaud, O. Emile, A. Aspect, and C. Cohen-Tannoudji, *Phys. Rev. Lett.* **72**, 203 (1994).
- [93] C. Leung, et al., To appear, .
- [94] G. Vidal, J. I. Latorre, E. Rico, and A. Kitaev, *Phys. Rev. Letters* **90** (2003).
- [95] S. Bravyi, *Quantum Info. Comput.* **5**, 216–238 (2005).
- [96] With a slight abuse of notation, we indicate the average over the gain/loss statistics with an overbar, as for the average over trajectories.